Author Manuscript
Faculty of Biology and Medicine Publication

This paper has been peer-reviewed but does not include the final publisher proof-corrections or journal pagination.

Published in final edited form as:

Title: Neuroinflammatory TNFα Impairs Memory via Astrocyte Signaling.

Authors: Habbas S, Santello M, Becker D, Stubbe H, Zappia G, Liaudet N, Klaus FR, Kollias G, Fontana A, Pryce CR, Suter T, Volterra A

Journal: Cell

Year: 2015 Dec 17

Volume: 163

Issue: 7

Pages: 1730-41

DOI: 10.1016/j.cell.2015.11.023

In the absence of a copyright statement, users should assume that standard copyright protection applies, unless the article contains an explicit statement to the contrary. In case of doubt, contact the journal publisher to verify the copyright status of an article.

UNIL | Université de Lausanne
Faculté de biologie et de médecine

Neuroinflammatory TNFα impairs memory via astrocyte signalling

Samia Habbas[1*], Mirko Santello[1*^], Denise Becker[1], Hiltrud Stubbe[1], Giovanna Zappia[1], Nicolas Liaudet[1], Federica R. Klaus[2], George Kollias[3], Adriano Fontana[4] , Christopher R. Pryce[2], Tobias Suter[5] & Andrea Volterra[1#]

[1]Department of Fundamental Neurosciences, University of Lausanne, Rue du Bugnon 9, 1005 Lausanne, Switzerland; [2]Department of Psychiatry, Psychotherapy and Psychosomatics, Psychiatric Hospital, University of Zurich, August Forel-Str. 7, 8008 Zurich, Switzerland; [3] B.S.R.C. "Alexander Fleming" 34 Fleming Street, 16672 Vari, Greece; [4]Institute of Experimental Immunology Inflammation and Sickness Behaviour, University of Zurich, Winterthurerstr. 190, 8057 Zurich, Switzerland; [5]Neuroimmunology and MS Research, University Hospital Zurich, Sternwartestr. 14, 8091 Zurich, Switzerland.

*These authors contributed equally to the study

#Corresponding author:
Andrea Volterra
Department of Fundamental Neurosciences,
University of Lausanne,
Rue du Bugnon 9,
1005 Lausanne, Switzerland
+41-21-6925271
Andrea.volterra@unil.ch

^Present address:
Department of Physiology
University of Bern
Bühlplatz 5, 3012 Bern
Switzerland

SUMMARY

The occurrence of cognitive disturbances upon CNS inflammation or infection has been correlated to increased levels of the cytokine tumour necrosis factor-α (TNFα). To-date, however, no specific mechanism via which this cytokine could alter cognitive circuits has been demonstrated. Here we show that local increase of TNFα in the hippocampal dentate gyrus activates astrocyte TNF receptor type 1 (TNFR1), which in turn triggers an astrocyte-neuron signaling cascade that results in persistent functional modification of hippocampal excitatory synapses. Astrocytic TNFR1 signaling is necessary for the hippocampal synaptic alteration and contextual learning-memory impairment observed in experimental autoimmune encephalitis (EAE), an animal model of Multiple Sclerosis (MS). This process may contribute to the pathogenesis of cognitive disturbances in MS as well as other CNS conditions accompanied by inflammatory states or infections.

INTRODUCTION

Synaptic activity is subject to various types of control, including regulatory inputs from surrounding glial cells. The release of gliotransmitters and factors from astrocytes induces synaptic modulation in cognitive circuits (reviewed in Araque et al. (2014)) and could contribute to cognitive function (Halassa et al., 2009; Han et al., 2012; Lee et al., 2014; Suzuki et al., 2011). An astrocyte-synapse modulatory pathway was described in the hippocampal dentate gyrus (DG) by which synaptically-activated astrocyte G protein-coupled receptors (GPCR) stimulate, via glutamate release, NR2B-containing NMDA receptors located in presynaptic excitatory fibers (pre-NMDAR, Jourdain et al. (2007)), resulting in transient strengthening of entorhinal cortex (EC)-hippocampal DG excitatory synapses (Jourdain et al., 2007), a circuit implicated in contextual learning and memory (Denny et al., 2014; Liu et al., 2012). Surprisingly, the glial regulatory pathway is itself controlled by the cytokine TNFα (Santello et al., 2011). Moreover, TNFα exerts additional controls at hippocampal synapses, such as on trafficking of AMPA (Beattie et al., 2002) and $GABA_A$ receptors (Pribiag and Stellwagen, 2013), emerging as a key physiological regulator of hippocampal synaptic function. Therefore, it is important to ask what happens to the hippocampal cognitive circuit when TNFα increases above local homeostatic levels (Santello and Volterra, 2012), as occurs in the CNS in a variety of medical conditions linked to inflammation or infection (Clark et al., 2010).

Observations in both humans and animals indicate a link between increased TNFα levels and cognitive alterations (Swardfager and Black, 2013; Yirmiya and Goshen, 2011), but data are descriptive and no study to date has identified the specific mechanisms. Here, starting from the identified characteristics of astrocytic modulation of DG synapses (Jourdain et al., 2007; Santello et al., 2011), and the specific observation that TNFα levels above a certain threshold

(>300 pM) trigger glutamate release from astrocytes (Bezzi et al., 2001; Domercq et al., 2006; Santello et al., 2011), we asked whether such a condition can affect excitatory transmission at perforant path-granule cell (PP-GC) hippocampal synapses. We find that high (600 pM) but not low (60 pM) TNFα concentrations persistently alter the functional properties of this synaptic circuit, acting via TNFR1 and a presynaptic mechanism involving NR2B-containing NMDAR. We also show that the same synaptic alteration, together with impaired contextual memory processing, is present in a murine model of multiple sclerosis (MS), a pathology often presenting with cognitive disturbances (Chiaravalloti and DeLuca, 2008). Finally, taking advantage of a transgenic mouse model, we directly demonstrate that both synaptic and cognitive impairments in the murine MS model depend to a large extent on activation of TNFR1 in astrocytes.

RESULTS

Increased TNFα persistently changes excitatory transmission in a hippocampal cognitive circuit.

To establish whether an increased local level of TNFα affects cognitive circuits, we initially compared the effects produced on excitatory EC-DG synapses by rapid (10 s) puffs of exogenous TNFα, applied at the estimated basal concentration (60 pM, Santello et al. (2011)) or at a 10-fold higher concentration (600 pM, **Fig. 1**). We used this experimental approach to evaluate the confined effects of the cytokine in the outer/middle dentate molecular layer (OML/MML, **Fig. 1A**), and to directly link the observed effect to the used concentration. Application of 60 pM TNFα did not produce any detectable change in basal synaptic activity (mean frequency, amplitude, and kinetics of AMPAR-dependent miniature post-synaptic excitatory currents (mEPSCs)) in dentate GCs within 30 min (**Fig. 1A-C** and Fig. **S1**). In

contrast, application of 600 pM TNFα produced progressive, strong increase in synaptic activity that reached plateau within 10 min and persisted unchanged after 30 min (and, in a few longer experiments, also after 50-60 min, data not shown). This long-lasting effect of the cytokine affected mEPSC frequency selectively, without changing mEPSC amplitude or kinetics (**Fig. 1A-C** and Fig. **S1A**), suggesting a presynaptic mechanism. When applied via prolonged bath incubation (1-2.5 h), 600 pM TNFα, however, in addition to mEPSC frequency, also increased mEPSC amplitude, albeit slightly (Fig. **S1B)**, suggesting that its action at excitatory synapses is both dose- and time-dependent. These recordings were performed in young mice (P17-25), but comparable effects were observed in adult animals (P60-90, **Fig. 1D**) ruling out that the TNFα effect is a developmental phenomenon. Increased mEPSC frequency in GCs predicts an enhanced EC drive to the DG. To verify this, we recorded EPSCs evoked by lateral PP stimulation (eEPSC) in individual GCs (**Fig. 1E-F**). Brief puffs of 600 pM TNFα, but not 60 pM, induced long-lasting increase in eEPSC amplitude and parallel change in short-term plasticity, denoted by reduced paired-pulse facilitation upon two consecutive stimuli. We conclude that high TNFα persistently enhances glutamate release probability at presynaptic PP terminals, thereby producing aberrant excitability of hippocampal GCs.

The TNFα effect requires activation of TNFR1 and ifenprodil-sensitive NMDAR

Given that TNFα above 300 pM triggers glutamate release from astrocytes and that astrocytic glutamate transiently strengthens GC synapses via activation of NR2B-containing pre-NMDAR (Bezzi et al., 2001; Jourdain et al., 2007; Santello et al., 2011), we tested whether the long-lasting synaptic effect of elevated TNFα was sensitive to the NR2B antagonist, ifenprodil. Indeed, in the presence of this drug, 600 pM TNFα failed to change mEPSC frequency (**Fig. 2A**). To then check whether TNFα activates NR2B-NMDAR persistently, we

applied ifenprodil at the peak of the synaptic effect of the cytokine. The NMDAR antagonist was now ineffective at reversing the TNFα increase in mEPSC frequency (**Fig. 2B**). Therefore, the long-lasting synaptic action of TNFα necessitates NR2B-NMDAR activation, but only during its induction. We next hypothesized a role for TNFR1, given that specific TNFR1 agonist antibodies mimic the glutamate-releasing action of TNFα in astrocytes (Bezzi et al., 2001). When we applied 600 pM TNFα to hippocampal slices from *tnfr1*$^{-/-}$ mice (Rothe et al., 1993), the cytokine failed to produce any increase in mEPSC frequency (**Fig. 2C**), although basal activity at GC synapses was normal (mEPSC frequency: wild-type: 1.63 ± 0.23 Hz (n = 11); *tnfr1*$^{-/-}$: 1.87 ± 0.28 (n = 4), p = 0.57; amplitude: wild-type: 7.91 ± 0.74 pA; *tnfr1*$^{-/-}$: 6.57 ± 0.57, p = 0.32, unpaired t-test). Taken together, these data confirm that TNFR1 plays a necessary role in the synaptic effect of TNFα and suggest that, at increased levels, the cytokine stimulates astrocyte signalling via this receptor.

tnfr1 knockout mice that conditionally re-express the receptor in astrocytes selectively

To establish that elevated TNFα indeed affects synaptic function via astrocyte signalling, we generated a new double transgenic mouse model, the *hGFAPcreT2/tnfr1*$^{cneo/cneo}$ mouse. To obtain this model we crossed mice with TNFR1 conditionally deleted in all cell types (*tnfr1*$^{cneo/cneo}$, Victoratos et al. (2006)), which behave as functional *tnfr1* knockout mice and lack any response to 600 pM TNFα at GC synapses (data not shown), with mice allowing TNFR1 re-expression selectively in astrocytes via tamoxifen (TAM)-inducible *cre* recombination driven by the human glial fibrillary acidic protein promoter (*hGFAPcreT2*, Hirrlinger et al. (2006), details in **Fig. 3A**). The efficiency and specificity of astrocytic recombination in the hippocampal DG was determined using *hGFAPcreT2/tnfr1*$^{cneo/cneo}$ mice expressing the ROSA-EYFP reporter (Srinivas et al., 2001) (**Fig. 3B**). Young (P22) and adult (P90) mice, studied 13 and 25 days after the first TAM injection, respectively, yielded similar

results. In 12 slices from 4 P90 mice we counted a total of 1680 $EYFP^+$ cells, most of which displayed the typical morphology of protoplasmic astrocytes and were distributed patchily, both in the dentate ML and in the hilus. These cells were also positive for the astrocytic marker glutamine synthetase (GS^+/$EYFP^+$ cells), and represented 37% of the total astrocytic population (GS^+ cells). About 10% of the $EYFP^+$ cells were confined to the subgranular zone (SGZ), most likely representing stem cells and neuronal precursors. In the MML/OML where PP-GC synapses lie, 99.3% (714 cells) of the $EYFP^+$ cells were GS^+, representing resident astrocytes, while 0.7% (5 cells) were $NeuN^+$ or GS^-, representing immature GCs sending growing dendrites. No reporter expression was detected in mice injected with corn oil (OIL), the TAM vehicle (Fig. **S2**), confirming that *cre* activity is specifically induced by TAM. The above results were corroborated by genomic PCR analysis of TAM-induced *tnfr1* recombination in FACS-sorted populations of $NeuN^+$ cells (no recombination) and $NeuN^-$ cells (prominent recombination) obtained from *hGFAPcreT2/tnfr1*$^{cneo/cneo}$ mouse brains (**Fig. 3C** and Fig. **S3**). Therefore, *hGFAPcreT2/tnfr1*$^{cneo/cneo}$ mice are a valid model to investigate the contribution of astrocyte signalling to the actions of TNFα.

Astrocyte-selective TNFR1 expression largely reconstitutes the synaptic effect of TNFα

We next investigated whether TNFα has an effect at PP-GC synapses in TAM-injected *hGFAPcreT2/tnfr1*$^{cneo/cneo}$ mice with TNFR1 expression functionally reconstituted selectively in astrocytes. Experiments were conducted 10-11 days after TAM onset. Puff of 600 pM TNFα locally in the MML/OML significantly increased mEPSC frequency in GCs (**Fig. 4A**). The cytokine effect was slow and persistent, as observed in wild-type mice (**Fig. 1B**), but less pronounced, possibly because only part of the astrocytic population re-expresses TNFR1 (**Fig. 3B**). In contrast, application of TNFα to slices from OIL-injected *hGFAPcreT2/tnfr1*$^{cneo/cneo}$ mice (global *tnfr1* knockouts, no TAM-induced recombination) produced no synaptic effect

(**Fig. 4B**). Any unspecific effect of TAM was also excluded, since in slices from TAM-injected *tnfr1*$^{cneo/cneo}$ mice, in which TAM cannot induce recombination, TNFα did not affect mEPSC activity (**Fig. 4C**). Therefore, expression of TNFR1 exclusively in GFAP-positive cells faithfully reproduces the persistent effect of TNFα on mEPSC frequency observed in wild-type mice.

Cognitive impairment accompanied by local inflammation and enhanced TNFα levels in the hippocampus in a mouse model of multiple sclerosis

Next we evaluated whether the identified astrocytic cascade triggered by high TNFα and causing persistent alteration of a cognitive synaptic circuit, is activated in a defined pathological condition and contributes to cognitive pathogenesis. We focused on multiple sclerosis (MS) because: (a) about 50% of MS patients suffer from cognitive disturbances (Chiaravalloti and DeLuca, 2008) and present anatomical/functional alterations in cognitive areas, including hippocampal DG (Gold et al., 2010); (b) in both MS patients and animal models of the pathology, notably experimental autoimmune encephalomyelitis (EAE), TNFα/TNFR1 signalling is implicated in pathogenesis (Eugster et al., 1999; Gregory et al., 2012; Kassiotis and Kollias, 2001). Our studies were performed in the EAE mouse model, using an adoptive transfer induction protocol (AT-EAE, Codarri et al. (2011); see Experimental Procedures), which allows the EAE CNS pathology to develop effectively also in TNFR1-deficient mice. We selected a cognitive test assessing functioning of the EC-DG circuitry, contextual fear conditioning (Anagnostaras et al., 2001; Denny et al., 2014; Liu et al., 2012) and investigated in adult C57BL/6J mice (P60-90) the effects of AT-EAE in its early phase (days 6 and 7 after transfer of autoimmune T cells (6-7 dpi), when classical EAE symptoms leading to ascending flaccid paralysis are absent (Fig. **S5**). An initial activity test (AT) excluded any confounding motor or emotional deficits due to AT-EAE (**Fig. 5A**).

Moreover, lack of effect on locomotor activity, freezing or rearing, indicated that motor function, exploration and normal anxiety state, respectively, were intact (Fig. **S6**). Subsequently, the mice underwent fear conditioning. Both control (sham-treated) and AT-EAE mice learned proficiently and acquired conditioned fear across the session, with AT-EAE mice showing a trend to lower freezing (**Fig. 5A**). The distance moved during electroshock was used as a measure of pain sensitivity and there was no effect of AT-EAE (Fig. **S6**). The next day we measured expression of long-term contextual memory. Only control mice exhibited the expected level of fear expression that they acquired on day 6. AT-EAE mice, in contrast, displayed a marked deficit in contextual memory (**Fig. 5A**). To investigate if this deficit was associated with the presence of a local pathology, we next performed immunohistochemistry experiments using leukocyte and microglia markers in hippocampal tissue (**Fig. 5B**). Compared to controls, AT-EAE mice (8-14 dpi) showed an accumulation of infiltrating leukocytes at the border between 3rd ventricle and DG and CA3 parenchyma. Moreover, within the parenchyma, microglia displayed the reactive phenotype, with enlarged cell bodies and shortened processes. The amount of reactive and/or infiltrating cells decreased progressively from the regions contacting the 3rd ventricle to the more distal ones, like CA1 and CA2. For simplicity, we refer to this pathology as "local inflammation". We also measured TNFα protein levels in punches of hippocampal tissue obtained (8 dpi) from the same mice studied in the contextual memory test (**Fig. 5C**). The local level of TNFα was increased 8-fold in AT-EAE mice compared to controls. The increase was specific to dorsal hippocampus, the region bordering the 3rd ventricle, which is integral to the contextual learning and memory circuitry (Anagnostaras et al., 2001). Therefore, at a stage of EAE that is fully asymptomatic in terms of motor pathology (8 dpi), mice present with overt local inflammatory pathology and enhanced TNFα levels in the hippocampus that could account for the observed contextual memory defect.

Altered hippocampal excitatory transmission in AT-EAE: protective effect of ifenprodil.

We next checked the state of the synaptic circuitry supporting contextual memory in AT-EAE mice (P60-90, 8-14 dpi). The paired-pulse ratio of eEPSCs at PP-GC synapses was significantly reduced compared to controls, indicative of an increased glutamate release from PP terminals. Consistently, the synaptic input-output relationship was altered, with significantly greater eEPSC amplitudes evoked by the same stimulation intensity (**Fig. 6A**). These defects strongly resemble those induced by high TNFα in younger mice (**Fig. 1E-F**). In keeping, AT-EAE mice also displayed significantly higher mEPSC activity in GCs than controls (**Fig. 6B**). The augmentation was most prominent in mEPSC frequency (34%), less pronounced in amplitude (16%), whereas kinetics were unchanged (rise-time: $p = 0.19$; decay-time: $p = 0.47$, ($n = 16$) unpaired t-test). Given that ifenprodil prevents the increase in mEPSC frequency induced by TNFα in young mice (**Fig. 2A**), we tested whether the drug was effective also in adult AT-EAE mice. In mice treated with ifenprodil *in vivo* during AT-EAE induction (see details in Supplementary Experimental Procedures), mEPSC frequency in GCs was lower than in untreated AT-EAE mice, and comparable to that in controls (**Fig. 6C)**. However, when ifenprodil was applied acutely to slices from untreated AT-EAE mice, the drug failed to decrease mEPSC frequency (before ifenprodil: 2.51 ± 0.16 Hz; after ifenprodil: 2.16 ± 0.18 Hz; $n = 8$; $p = 0.09$, paired t-test). These data suggest that NR2B-containing NMDAR participate in the induction (but not maintenance) of the persistent change of PP-GC excitatory transmission induced by AT-EAE. Intriguingly, the *in vivo* treatment with ifenprodil did not counteract the mEPSC amplitude increase observed in AT-EAE mice (**Fig. 6C**), suggesting that this component of the synaptic change is NR2B-independent.

Causal role of astrocyte TNFR1 signaling in the hippocampal synaptic alterations and cognitive impairment induced by AT-EAE.

To determine whether the synaptic changes observed in AT-EAE mice depend on TNFα acting via astrocyte TNFR1 signalling, we next induced AT-EAE in TAM- or OIL-treated adult *hGFAPcreT2/tnfr1*$^{cneo/cneo}$ mice (See Experimental Procedures for temporal details). mEPSC frequency in GCs of TAM-treated AT-EAE mice (astrocyte TNFR1 re-expression) was significantly higher than in their OIL-treated counterparts (**Fig. 7A**) and similar to that seen in wild-type AT-EAE mice (**Fig. 7B**, p = 0.1, unpaired t-test). mEPSC amplitude did not differ, however, from that of wild-type AT-EAE mice (p = 0.14, ANOVA followed by post-hoc comparisons). The effect on mEPSC frequency was not due to TAM *per se*, because TAM-treated AT-EAE *tnfr1*$^{cneo/cneo}$ mice (no recombination) did not show any increased mEPSC frequency (**Fig. 7B**). All four transgenic groups developed a similar pattern of local inflammation in the hippocampal DG, apparently indistinguishable from that seen in wild-type AT-EAE mice (compare **Figs. 7C** and **5B**), indicating that the TNFR1-dependent synaptic changes are triggered downstream of the local inflammatory reaction. To investigate whether astrocyte TNFR1 signalling is also responsible for impaired contextual memory in AT-EAE mice, we studied three groups of AT-EAE mice: TAM- or OIL-treated *hGFAPcreT2/tnfr1*$^{cneo/cneo}$ and TAM-treated *tnfr1*$^{cneo/cneo}$. At 5 dpi, mice were given an open field test which excluded any group difference in behaviours relevant to motor function, anxiety and exploration (Fig. **S7**). At 6 dpi, contextual fear conditioning was conducted. All three groups demonstrated acquisition of freezing **(Fig. 7D**), with OIL-treated *hGFAPcreT2/tnfr1*$^{cneo/cneo}$ mice and TAM-treated *tnfr1*$^{cneo/cneo}$ mice exhibiting a similar amount of conditioning, consistent with the absence of any TAM effect. TAM-treated *hGFAPcreT2/tnfr1*$^{cneo/cneo}$ mice exhibited proportionally less acquisition of freezing relative to the other two groups. This deficit was not due to reduced sensitivity to the electroshock

because all groups moved the same distance during electroshock (Fig. **S7**). At 7 dpi, mice were tested for fear expression. TAM-treated *hGFAPcreT2/tnfr1*$^{cneo/cneo}$ mice showed a trend to decreased freezing relative to the other two groups (**Fig. 7D**, middle), which was proportional to the decreased fear acquisition of the previous day. At 8 dpi, in a second fear expression test, TAM-treated *hGFAPcreT2/tnfr1*$^{cneo/cneo}$ mice exhibited further reduction of fear expression and significantly less expression than the two other groups (**Fig. 7D**, right). These data indicate a cognitive phenotype in TAM-treated *hGFAPcreT2/tnfr1*$^{cneo/cneo}$ mice similar to that observed in wild-type AT-EAE mice although the latter presented lower initial learning deficit and faster-onset memory deficit, differences that could be due to intrinsic variability of the AT-EAE protocol across experiments. We exclude other confounding factors because a second open field test conducted at 9 dpi confirmed lack of locomotor and exploratory behavioural differences between groups (data not shown). We conclude that astrocyte TNFR1 expression is required for both functional alteration of the EC-DG synaptic circuit and contextual learning and memory deficit in AT-EAE mice.

DISCUSSION

Our study links a local increase in TNFα in the hippocampus to synaptic and cognitive dysfunction via astrocyte signalling. This astrocytic pathway is activated in EAE, an animal model of multiple sclerosis, and is necessary for the development of the contextual memory deficit observed and thus its delineation may reveal new therapeutic targets against cognitive decline (discussed below).

Astrocyte TNFR1 is required for induction of synaptic and cognitive defects.

In EAE, activated microglia and infiltrating macrophages controlled by CD4+ T cells are the most likely cause of local TNFα increase in the DG (**Fig. 5B**; Renno et al. (1995)), whereas downstream activation of TNFR1 in astrocytes appears to be the critical event for induction of the core synaptic and behavioural phenotype. This is demonstrated by reconstitution of the phenotype in *hGFAPcreT2/tnfr1*$^{cneo/cneo}$ mice, functional *tnfr1* knockouts in which TNFR1, via TAM-induced *cre* recombination, is re-expressed exclusively in GFAP-positive cells. Astrocytes represent the only population of such cells that we observed at the time of our experiments (10-22 days from the start of recombination) in the dentate OML/MML where excitatory PP-GC synapses are located. Recombination in the DG occurs also in the much smaller population of SGZ neural stem cells, but expression of TNFR1 in these cells and in the derived neuronal precursors and immature GCs very unlikely contributes to the TNFα-dependent phenotype because: (a) different from astrocytes, these cells lie distally from PP-GC synapses (25 days after the start of recombination those with growing dendrites able to reach the OML/MML were 0.7% of the resident astrocytic population undergoing recombination); (b) full integration of newborn GCs into the excitatory network as mature GCs requires 8 weeks (Toni et al., 2007), and in any case these cells may contribute to contextual memory formation only after 4 weeks of maturation (Gu et al., 2012), a time-frame incompatible with the timing of our experiments.

Pathological TNFα contributes to the synaptic alterations: signaling mechanism

TNFα produces persistent change in excitatory transmission only when its concentration increases up to levels that are specific to pathological states. In the early phases of AT-EAE, we measured an 8-fold increase in tissue TNFα levels in the dorsal hippocampus. This increase resembles in proportion the 10-fold increase that we used to mimic pathological (600 pM) versus physiological (60 pM) TNFα levels when applying the exogenous cytokine locally

in the DG. In absolute value, 600 pM could represent a concentration close to the one reached by the cytokine during EAE, because at this concentration exogenous TNFα produced synaptic changes very similar, in both quality and quantity, to those observed in AT-EAE mice. While this value is much higher than the tissue concentration that we measured, it could mimic the TNFα concentration sensed by astrocytes locally, which may be orders of magnitude higher than the average concentration in the tissue (Wang et al., 2011). Regardless, 600 pM exogenous TNFα and the endogenous cascade operating in AT-EAE appear to act via the same mechanism, as both enhance mEPSC frequency via astrocyte TNFR1 and an ifenprodil-sensitive mechanism. The latter data strongly suggests that TNFα activates at PP-GC synapses the same pathway triggered by astrocyte GPRC agonists in physiological conditions, eventually resulting in stimulation of NR2B-containing pre-NMDAR (Jourdain et al., 2007; Santello et al., 2011), although the TNFα-induced activation must be different because it leads to long-lasting and irreversible modifications of synaptic activity. TNFα (upon prolonged incubation in normal mice) and the endogenous cascade of AT-EAE produce another common effect, a small increase in mEPSC amplitude. This effect is ifenprodil-insensitive, and therefore mechanistically different from the astrocyte-mediated effect, which is clearly presynaptic. It could be, in contrast, post-synaptic, consistent with the reported capacity of TNFα to promote surface insertion of AMPAR subunits at dendritic spines via stimulation of neuronal TNFR1 (Stellwagen et al., 2005). The contribution of this latter mechanism to the synaptic and cognitive phenotype in AT-EAE remains to be defined given the substantial restoration of the phenotype upon TNFR1 re-expression selectively in astrocytes.

Local malfunction of the entorhinal cortex-hippocampal excitatory circuit

The TNFα/TNFR1-dependent synaptic changes identified here lead to alteration of the input-output relationship in the EC-DG circuit, which is critically involved in contextual memory processing (Liu et al., 2012; Denny et al, 2014). Accordingly, we find altered contextual learning and memory performance in AT-EAE mice with increased TNFα levels in dorsal hippocampus. A persistently increased excitatory drive may reduce the dynamic range and impair long-term potentiation (LTP) (Goussakov et al., 2000; Pascual et al., 2005), a defect already observed in the DG with TNFα concentrations similar to those used in this study (Cunningham et al., 1996), and likely to cause abnormal processing of learning and memory-related information (Chapman et al., 1999; Tombaugh et al., 2002). Definitive proof of the causative role played by the observed synaptic alterations could be achieved by reducing the abnormal excitatory PP input to GCs in AT-EAE mice in vivo, e.g. optogenetically, and showing consequent amelioration of the cognitive deficit. Such deficit appears in temporal overlap with a local inflammation pathology restricted to the hippocampal areas surrounding the 3rd ventricle, notably the DG (**Fig 5B**, large field). This suggests that the cognitive phenotype is locally-generated and not due to a generalized inflammatory state of the brain, although it does not exclude other sites of local inflammation in other brain regions at these stages of the pathology (Haji et al., 2012), nor that other behavioral processes, e.g. auditory fear, might be impacted (Acharjee et al., 2013). Putting all the above data together, we propose that a causal chain links EAE local inflammation to synaptic alteration and cognitive dysfunction via the action of TNFα and its astrocyte TNFR1. In this context, our data bring together a number of sparse recent observations suggesting that TNFα is involved in the synaptic alterations observed in EAE and other CNS pathology models (Centonze et al., 2009; Haji et al., 2012; Xu et al., 2010; Yang et al., 2013) and that enhanced TNFα levels are associated with the manifestation of cognitive defects (Belarbi et al., 2012; Gabbita et al.,

2012; Terrando et al., 2010, reviewed in Clark et al. 2010; Swardfager and Black 2013; but see Han et al. 2013).

Relevance for cognitive dysfunction in MS and other medical conditions

While cognitive disturbances involving hippocampal alterations (Gold et al., 2010) affect a large number of MS patients (Chiaravalloti and DeLuca, 2008), the responsible mechanisms have remained elusive. The present findings provide a plausible mechanistic basis and also suggest that the mechanism responsible for cognitive dysfunction is distinct from the one causing the motor symptoms. In addition to MS, our findings may be relevant to other CNS pathologies characterized by cognitive disturbances and elevated grey matter TNFα levels, notably Alzheimer's disease (McAlpine and Tansey, 2008; AD). Indeed, in animal models of AD, TNFα signaling via TNFR1 has been implicated in learning and memory deficits (He et al., 2007). Other inflammatory states due to bacterial or viral infections directly affecting the CNS, and even peripheral inflammatory states that result in septic encephalopathy are accompanied by cognitive disturbances (Clark et al., 2010; Swardfager and Black, 2013). They could therefore present synaptic alterations similar to those recognized in AT-EAE mice, caused by the identified astrocytic pathway. In view of these considerations, therapeutic agents targeting the described signaling steps, specifically astrocytic TNFR1 and pre-NMDAR, could be tested against cognitive disturbances in the above medical conditions. TNFR1 has been strongly implicated in the pathogenesis of MS (Gregory et al., 2012) and EAE (Kassiotis and Kollias, 2001), but not yet in the cognitive aspects. According to animal studies and recent clinical trials selective blockade of TNFR1 function represents a promising therapeutic strategy in MS (Van Hauwermeiren et al., 2011). Development of TNFR1 antagonists with central action could offer the important additional advantage of tackling the cognitive component of the pathology. As for pre-NMDAR, at hippocampal synapses these

receptors contain the NR2B subunit (Jourdain et al., 2007). NR2B antagonists are currently under clinical investigation in several neurologic and psychiatric disorders (Paoletti et al., 2013). For effective use against cognitive impairment in MS and other conditions, more selective "presynaptic NR2B agents" or agents acting on other subunits typical of pre-NMDAR (Larsen et al., 2011) should, however, be developed.

EXPERIMENTAL PROCEDURES

Animal models

tnfr1$^{-/-}$ mice (Rothe et al., 1993), *tnfr1*$^{cneo/cneo}$ mice (Victoratos et al., 2006) and *hGFAPcreT2* mice (Hirrlinger et al., 2006) expressing a conditional EYFP reporter in the ROSA locus (Srinivas et al., 2001), all on C57BL/6 background, were generated and maintained as described in the original studies. The latter two lines were cross-bred to generate *hGFAPcreT2/tnfr1*$^{cneo/cneo}$ mice. To achieve gene recombination, *hGFAPcreT2/tnfr1*$^{cneo/cneo}$ and *tnfr1*$^{cneo/cneo}$ mice were administered TAM (100 mg/kg) dissolved in corn oil (OIL), or OIL alone as a control carrier, once per day for 8 consecutive days (Hirrlinger et al., 2006). For AT-EAE induction, mice were injected with effector MOG35-55-specific CD4+ T cells generated from 2D2 mice (details in Codarri et al. (2011)). Intervals from the first TAM or OIL injection were: 10-12 days in electrophysiology experiments without AT-EAE induction; 16-22 days if AT-EAE was induced; 13-16 days in behaviour experiments in AT-EAE mice; 13 days (young mice) and 25 days (adult mice) in immunohistochemistry experiments looking at EYFP reporter expression; 16-22 days in the same experiments looking at inflammation markers.

Electrophysiology experiments

Patch-clamp recordings were performed in acute brain horizontal slices at excitatory PP-GC synapses in the hippocampal DG. GCs were patched with borosilicate glass pipettes (3-5 MΩ) and voltage-clamped at –65 mV. All experiments were carried out at 34ºC in the presence of picrotoxin (100 µM), to block $GABA_A$ receptor-mediated currents. To study mEPSC activity in isolation, tetrodotoxin (TTX, 1 µM) was added to block action potentials. To test the effect of TNFα (60-600 pM), the cytokine was locally applied via an ejection pipette positioned in the OML by using a single 10 s pulse (4-7 psi) delivered by a PV830 Pneumatic PicoPump (WPI, Germany). In some experiments we indirectly verified spatial diffusion and rapid washout of TNFα by co-ejecting Cascade blue, a fluorescent dye, under two-photon imaging. Recordings in each GC started about 10 min after reaching whole-cell and covered a period going from 5 min before to 30 min after TNFα application. Stimulation of the PP was done with a theta electrode placed in the OML. Recordings were analyzed essentially as described in Jourdain et al. (2007) and Santello et al. (2011).

Immunohistochemistry

For immunofluorescence staining, 50-µm-thick horizontal slices were prepared from fixed brains by use of a cryo-microtome (Microm International AG). After permeabilization, slices were incubated with primary antibodies (72 h, 4°C) and then with secondary antibodies in 0.3% triton-X 100/PBS (2h, room temperature) and with 4′,6-diamidino-2-phenylindole (DAPI, 300 nM) to label nuclei. Large field images in the hippocampus and neighboring regions were acquired using a Leica MZ16FA stereomicroscope (Leica Microsystems, Germany) equipped with Leica EL6000 illumination. In all other cases, images were acquired with a Leica SP5 AOBS confocal microscope (Leica Microsystems, Germany), using a 40x oil immersion “HCX PL APO” objective (NA: 1.25-0.75). Analysis was done with ImageJ software (NIH, USA).

Behavioural experiments

Acquisition of contextual fear conditioning followed 24 h later by a test of its expression (sometimes repeated at 48h) were used as tests of, respectively, contextual learning and memory. The fear conditioning test, in some cases preceded by an open field test the day before, was carried out using a fear conditioning arena (context) with a grid floor which could be electrified, placed within an isolation chamber (Ugo Basile, Italy) controlled by Ethovision XT software (Noldus, Netherlands). Mice were first given a 5-min activity test (AT) without electroshocks to assess locomotor activity, baseline freezing and rearing. Next the conditioning session comprised six inescapable electroshocks (0.20 mA x 2 s each), delivered at 2 min intervals. After this test, mice were returned to their home cages until the following day, when they were placed back in the same arena in the absence of electroshocks for the mnemonic fear expression test. Mice were considered to be freezing if no movement was detected for at least 2 s and the measure was expressed as a percentage of time spent freezing.

A detailed description of all experimental methods is provided in the Supplemental Experimental Procedures.

AUTHOR CONTRIBUTIONS

SH performed and analyzed electrophysiology, two-photon imaging, flow cytometry sorting, PCR, and contributed to immunohistochemistry, image analysis, measure of tissue TNFα and statistical analysis; MS performed and analyzed electrophysiology and contributed to development of *hGFAPcreT2/tnfr1*$^{cneo/cneo}$ mouse line, design of electrophysiology experiments in AT-EAE mice and immunohistochemistry; DB performed and analyzed behavioural experiments in transgenic AT-EAE mice; HS generated and maintained the transgenic lines and performed immunohistochemistry; GZ performed immunohistochemistry; NL performed image and statistical analyses; FK contributed to

behavioural experiments and measure of tissue TNFα; GK contributed to development of *hGFAPcreT2/tnfr1*$^{cneo/cneo}$ mouse line, design of PCR primers and provided advice; AF advised on design of AT-EAE experiments; CRP designed and performed behavioural experiments on wild-type mice, supervised behavioural experiments on transgenic mice, and contributed to measure of tissue TNFα; TS designed and performed *in vivo* AT-EAE protocols including animals scoring, and contributed to design of experiments in AT-EAE animals; AV supervised and coordinated the project and wrote the manuscript with the support of all the authors.

ACKNOWLEDGMENTS

We thank G. Stocca and H. Sigrist for help in two photon imaging and in AT-EAE fear conditioning experiments, respectively; N. Nevian for biocytin staining; I. Savtchouk for comments to the manuscript; F. Kirchhoff for providing *hGFAPcreT2* mice; T. Nevian for providing access to his lab equipment for some electrophysiology experiments. E. Seifritz for support and expert advice on the translational study of behavioural pathology. This work was supported by the ERC Advanced grant 340368 "Astromnesis" and by grants from the Swiss National Science Foundation (SNSF) 31003A–140999, NCCR "Synapsy" and NCCR "Transcure" to AV and from the SNSF (31003A-141137) to CRP. SH received a post-doctoral fellowship from NCCR "Synapsy"; MS received a PhD fellowship from FBM, University of Lausanne. FRK received an MD-PhD fellowship from the SNSF; AF is a Senior Research Professor for Neuroscience of the Gemeinnützige Hertie Stiftung; TS is supported by the Clinical Research Priority Program Multiple Sclerosis of the University of Zurich.

REFERENCES

Acharjee, S., Nayani, N., Tsutsui, M., Hill, M.N., Ousman, S.S., and Pittman, Q.J. (2013). Altered cognitive-emotional behavior in early experimental autoimmune encephalitis--cytokine and hormonal correlates. Brain, behavior, and immunity *33*, 164-172.

Anagnostaras, S.G., Gale, G.D., and Fanselow, M.S. (2001). Hippocampus and contextual fear conditioning: recent controversies and advances. Hippocampus *11*, 8-17.

Araque, A., Carmignoto, G., Haydon, P.G., Oliet, S.H., Robitaille, R., and Volterra, A. (2014). Gliotransmitters travel in time and space. Neuron *81*, 728-739.

Beattie, E.C., Stellwagen, D., Morishita, W., Bresnahan, J.C., Ha, B.K., Von Zastrow, M., Beattie, M.S., and Malenka, R.C. (2002). Control of synaptic strength by glial TNFalpha. Science *295*, 2282-2285.

Belarbi, K., Jopson, T., Tweedie, D., Arellano, C., Luo, W., Greig, N.H., and Rosi, S. (2012). TNF-alpha protein synthesis inhibitor restores neuronal function and reverses cognitive deficits induced by chronic neuroinflammation. J Neuroinflammation *9*, 23.

Bezzi, P., Domercq, M., Brambilla, L., Galli, R., Schols, D., De Clercq, E., Vescovi, A., Bagetta, G., Kollias, G., Meldolesi, J., *et al.* (2001). CXCR4-activated astrocyte glutamate release via TNFalpha: amplification by microglia triggers neurotoxicity. Nat Neurosci *4*, 702-710.

Centonze, D., Muzio, L., Rossi, S., Cavasinni, F., De Chiara, V., Bergami, A., Musella, A., D'Amelio, M., Cavallucci, V., Martorana, A., *et al.* (2009). Inflammation triggers synaptic alteration and degeneration in experimental autoimmune encephalomyelitis. J Neurosci *29*, 3442-3452.

Chapman, P.F., White, G.L., Jones, M.W., Cooper-Blacketer, D., Marshall, V.J., Irizarry, M., Younkin, L., Good, M.A., Bliss, T.V., Hyman, B.T., *et al.* (1999). Impaired synaptic plasticity and learning in aged amyloid precursor protein transgenic mice. Nat Neurosci *2*, 271-276.

Chiaravalloti, N.D., and DeLuca, J. (2008). Cognitive impairment in multiple sclerosis. Lancet Neurol *7*, 1139-1151.

Clark, I.A., Alleva, L.M., and Vissel, B. (2010). The roles of TNF in brain dysfunction and disease. Pharmacol Ther *128*, 519-548.

Codarri, L., Gyulveszi, G., Tosevski, V., Hesske, L., Fontana, A., Magnenat, L., Suter, T., and Becher, B. (2011). RORgammat drives production of the cytokine GM-CSF in helper T cells, which is essential for the effector phase of autoimmune neuroinflammation. Nat Immunol *12*, 560-567.

Cunningham, A.J., Murray, C.A., O'Neill, L.A., Lynch, M.A., and O'Connor, J.J. (1996). Interleukin-1 beta (IL-1 beta) and tumour necrosis factor (TNF) inhibit long-term potentiation in the rat dentate gyrus in vitro. Neurosci Lett *203*, 17-20.

Denny, C.A., Kheirbek, M.A., Alba, E.L., Tanaka, K.F., Brachman, R.A., Laughman, K.B., Tomm, N.K., Turi, G.F., Losonczy, A., and Hen, R. (2014). Hippocampal memory traces are differentially modulated by experience, time, and adult neurogenesis. Neuron *83*, 189-201.

Domercq, M., Brambilla, L., Pilati, E., Marchaland, J., Volterra, A., and Bezzi, P. (2006). P2Y1 receptor-evoked glutamate exocytosis from astrocytes: control by tumor necrosis factor-alpha and prostaglandins. J Biol Chem *281*, 30684-30696.

Eugster, H.P., Frei, K., Bachmann, R., Bluethmann, H., Lassmann, H., and Fontana, A. (1999). Severity of symptoms and demyelination in MOG-induced EAE depends on TNFR1. Eur J Immunol *29*, 626-632.

Gabbita, S.P., Srivastava, M.K., Eslami, P., Johnson, M.F., Kobritz, N.K., Tweedie, D., Greig, N.H., Zemlan, F.P., Sharma, S.P., and Harris-White, M.E. (2012). Early intervention with a small molecule inhibitor for tumor necrosis factor-alpha prevents cognitive deficits in a triple transgenic mouse model of Alzheimer's disease. J Neuroinflammation *9*, 99.

Gold, S.M., Kern, K.C., O'Connor, M.F., Montag, M.J., Kim, A., Yoo, Y.S., Giesser, B.S., and Sicotte, N.L. (2010). Smaller cornu ammonis 2-3/dentate gyrus volumes and elevated cortisol in multiple sclerosis patients with depressive symptoms. Biol Psychiatry *68*, 553-559.

Goussakov, I.V., Fink, K., Elger, C.E., and Beck, H. (2000). Metaplasticity of mossy fiber synaptic transmission involves altered release probability. J Neurosci *20*, 3434-3441.

Gregory, A.P., Dendrou, C.A., Attfield, K.E., Haghikia, A., Xifara, D.K., Butter, F., Poschmann, G., Kaur, G., Lambert, L., Leach, O.A., *et al.* (2012). TNF receptor 1 genetic risk mirrors outcome of anti-TNF therapy in multiple sclerosis. Nature *488*, 508-511.

Gu Y, Arruda-Carvalho M, Wang J, Janoschka SR, Josselyn SA, Frankland PW, Ge S. (2012). Optical controlling reveals time-dependent roles for adult-born dentate granule cells. Nat Neurosci. *15*,1700-6.Haji, N., Mandolesi, G., Gentile, A., Sacchetti, L., Fresegna, D.,

Rossi, S., Musella, A., Sepman, H., Motta, C., Studer, V., *et al.* (2012). TNF-alpha-mediated anxiety in a mouse model of multiple sclerosis. Exp Neurol *237*, 296-303.

Halassa, M.M., Florian, C., Fellin, T., Munoz, J.R., Lee, S.Y., Abel, T., Haydon, P.G., and Frank, M.G. (2009). Astrocytic modulation of sleep homeostasis and cognitive consequences of sleep loss. Neuron *61*, 213-219.

Han, J., Kesner, P., Metna-Laurent, M., Duan, T., Xu, L., Georges, F., Koehl, M., Abrous, D.N., Mendizabal-Zubiaga, J., Grandes, P., *et al.* (2012). Acute cannabinoids impair working memory through astroglial CB1 receptor modulation of hippocampal LTD. Cell *148*, 1039-1050.

Han, X., Chen, M., Wang, F., Windrem, M., Wang, S., Shanz, S., Xu, Q., Oberheim, N.A., Bekar, L., Betstadt, S., *et al.* (2013). Forebrain engraftment by human glial progenitor cells enhances synaptic plasticity and learning in adult mice. Cell Stem Cell *12*, 342-353.

He, P., Zhong, Z., Lindholm, K., Berning, L., Lee, W., Lemere, C., Staufenbiel, M., Li, R., and Shen, Y. (2007). Deletion of tumor necrosis factor death receptor inhibits amyloid beta generation and prevents learning and memory deficits in Alzheimer's mice. J Cell Biol *178*, 829-841.

Hirrlinger, P.G., Scheller, A., Braun, C., Hirrlinger, J., and Kirchhoff, F. (2006). Temporal control of gene recombination in astrocytes by transgenic expression of the tamoxifen-inducible DNA recombinase variant CreERT2. Glia *54*, 11-20.

Jourdain, P., Bergersen, L.H., Bhaukaurally, K., Bezzi, P., Santello, M., Domercq, M., Matute, C., Tonello, F., Gundersen, V., and Volterra, A. (2007). Glutamate exocytosis from astrocytes controls synaptic strength. Nat Neurosci *10*, 331-339.

Kassiotis, G., and Kollias, G. (2001). Uncoupling the proinflammatory from the immunosuppressive properties of tumor necrosis factor (TNF) at the p55 TNF receptor level: implications for pathogenesis and therapy of autoimmune demyelination. J Exp Med *193*, 427-434.

Larsen, R.S., Corlew, R.J., Henson, M.A., Roberts, A.C., Mishina, M., Watanabe, M., Lipton, S.A., Nakanishi, N., Perez-Otano, I., Weinberg, R.J., *et al.* (2011). NR3A-containing NMDARs promote neurotransmitter release and spike timing-dependent plasticity. Nat Neurosci *14*, 338-344.

Lee, H.S., Ghetti, A., Pinto-Duarte, A., Wang, X., Dziewczapolski, G., Galimi, F., Huitron-Resendiz, S., Pina-Crespo, J.C., Roberts, A.J., Verma, I.M., *et al.* (2014). Astrocytes contribute to gamma oscillations and recognition memory. Proc Natl Acad Sci U S A *111*, E3343-3352.

Liu, X., Ramirez, S., Pang, P.T., Puryear, C.B., Govindarajan, A., Deisseroth, K., and Tonegawa, S. (2012). Optogenetic stimulation of a hippocampal engram activates fear memory recall. Nature *484*, 381-385.

McAlpine, F.E., and Tansey, M.G. (2008). Neuroinflammation and tumor necrosis factor signaling in the pathophysiology of Alzheimer's disease. J Inflamm Res *1*, 29-39.

Paoletti, P., Bellone, C., and Zhou, Q. (2013). NMDA receptor subunit diversity: impact on receptor properties, synaptic plasticity and disease. Nat Rev Neurosci *14*, 383-400.

Pascual, O., Casper, K.B., Kubera, C., Zhang, J., Revilla-Sanchez, R., Sul, J.Y., Takano, H., Moss, S.J., McCarthy, K., and Haydon, P.G. (2005). Astrocytic purinergic signaling coordinates synaptic networks. Science *310*, 113-116.

Pribiag, H., and Stellwagen, D. (2013). TNF-alpha downregulates inhibitory neurotransmission through protein phosphatase 1-dependent trafficking of GABA(A) receptors. J Neurosci *33*, 15879-15893.

Renno, T., Krakowski, M., Piccirillo, C., Lin, J.Y., and Owens, T. (1995). TNF-alpha expression by resident microglia and infiltrating leukocytes in the central nervous system of mice with experimental allergic encephalomyelitis. Regulation by Th1 cytokines. J Immunol *154*, 944-953.

Rothe, J., Lesslauer, W., Lotscher, H., Lang, Y., Koebel, P., Kontgen, F., Althage, A., Zinkernagel, R., Steinmetz, M., and Bluethmann, H. (1993). Mice lacking the tumour necrosis factor receptor 1 are resistant to TNF-mediated toxicity but highly susceptible to infection by Listeria monocytogenes. Nature *364*, 798-802.

Santello, M., Bezzi, P., and Volterra, A. (2011). TNFalpha controls glutamatergic gliotransmission in the hippocampal dentate gyrus. Neuron *69*, 988-1001.

Santello, M., and Volterra, A. (2012). TNFalpha in synaptic function: switching gears. Trends Neurosci *35*, 638-647.

Srinivas, S., Watanabe, T., Lin, C.S., William, C.M., Tanabe, Y., Jessell, T.M., and Costantini, F. (2001). Cre reporter strains produced by targeted insertion of EYFP and ECFP into the ROSA26 locus. BMC Dev Biol *1*, 4.

Stellwagen, D., Beattie, E.C., Seo, J.Y., and Malenka, R.C. (2005). Differential regulation of AMPA receptor and GABA receptor trafficking by tumor necrosis factor-alpha. J Neurosci *25*, 3219-3228.

Suzuki, A., Stern, S.A., Bozdagi, O., Huntley, G.W., Walker, R.H., Magistretti, P.J., and Alberini, C.M. (2011). Astrocyte-neuron lactate transport is required for long-term memory formation. Cell *144*, 810-823.

Swardfager, W., and Black, S.E. (2013). Dementia: A link between microbial infection and cognition? Nat Rev Neurol *9*, 301-302.

Terrando, N., Monaco, C., Ma, D., Foxwell, B.M., Feldmann, M., and Maze, M. (2010). Tumor necrosis factor-alpha triggers a cytokine cascade yielding postoperative cognitive decline. Proc Natl Acad Sci U S A *107*, 20518-20522.

Tombaugh, G.C., Rowe, W.B., Chow, A.R., Michael, T.H., and Rose, G.M. (2002). Theta-frequency synaptic potentiation in CA1 in vitro distinguishes cognitively impaired from unimpaired aged Fischer 344 rats. J Neurosci *22*, 9932-9940.

Toni, N., Teng, E.M., Bushong, E.A., Aimone, J.B., Zhao, C., Consiglio, A., van Praag, H., Martone, M.E., Ellisman, M.H., and Gage, F.H. (2007). Synapse formation on neurons born in the adult hippocampus. Nat Neurosci *10*, 727-734.

Van Hauwermeiren, F., Vandenbroucke, R.E., and Libert, C. (2011). Treatment of TNF mediated diseases by selective inhibition of soluble TNF or TNFR1. Cytokine Growth Factor Rev *22*, 311-319.

Victoratos, P., Lagnel, J., Tzima, S., Alimzhanov, M.B., Rajewsky, K., Pasparakis, M., and Kollias, G. (2006). FDC-specific functions of p55TNFR and IKK2 in the development of FDC networks and of antibody responses. Immunity *24*, 65-77.

Wang, S., Ota, S., Guo, B., Ryu, J., Rhodes, C., Xiong, Y., Kalim, S., Zeng, L., Chen, Y., Teitell, M.A., *et al.* (2011). Subcellular resolution mapping of endogenous cytokine secretion by nano-plasmonic-resonator sensor array. Nano Lett *11*, 3431-3434.

Xu, Z.Z., Zhang, L., Liu, T., Park, J.Y., Berta, T., Yang, R., Serhan, C.N., and Ji, R.R. (2010). Resolvins RvE1 and RvD1 attenuate inflammatory pain via central and peripheral actions. Nat Med *16*, 592-597, 591p following 597.

Yang, G., Parkhurst, C.N., Hayes, S., and Gan, W.B. (2013). Peripheral elevation of TNF-alpha leads to early synaptic abnormalities in the mouse somatosensory cortex in experimental autoimmune encephalomyelitis. Proc Natl Acad Sci U S A *110*, 10306-10311.

Yirmiya, R., and Goshen, I. (2011). Immune modulation of learning, memory, neural plasticity and neurogenesis. Brain Behav Immun *25*, 181-213.

FIGURE LEGENDS

Figure 1: *Concentration-Dependent Effects of Exogenous TNFα on Excitatory Synaptic Activity in a Hippocampal Cognitive Circuit.* **A**, **left:** two-photon image of the experimental setting for local TNFα application in the hippocampal DG (GC: green, Alexa-488; astrocytes: red, sulforhodamine 101; TNFα diffusion upon 10s local puff: Cascade blue with dotted white contour). Scale bar: 20 µm; GCL = granule cell layer; IML, MML and OML = inner, middle and outer molecular layer, respectively. **A, right:** representative traces of mEPSC activity in control condition (grey) and 30 min after puffing 60 pM TNFα (azure) or 600 pM TNFα (red); scale bars: 20 s, 20 pA. Insets: representative mEPSC events for each condition taken at the indicated time (triangle); scale bars: 10 ms, 5 pA. **B, left**: histograms of mean mEPSC frequency in control condition (n = 16) and 30 min after puffing 60 pM TNFα (n = 5) or 600 pM TNFα (n =11). Only the latter treatment increases mEPSC frequency vs. control ($p<0.001$, ANOVA followed by post hoc comparisons: ANOVA + phc). **B, middle:** representative cumulative probability plots comparing mEPSC inter-event intervals (IEI) in the above conditions. **B, right**: mEPSC activity monitored from 5 min before puffing TNFα (puff denoted by arrow) to 30 min after puffing; azure: 60 pM TNFα; red: 600 pM TNFα. Only the latter increases mEPSC frequency (repeated measures ANOVA + phc: at 3, 5, 15 and 30 min: $p<0.01$; at 10, 20 and 25 min: $p<0.001$). **C**: histograms (**left**) and cumulative probability plots (**right**) of mean mEPSC amplitude before (control) and 30 min after application of 60 pM or 600 pM TNFα. Neither TNFα concentration produced an effect ($p>0.1$, ANOVA). **D:** comparison of the effect of 600 pM TNFα in young (n = 11) and adult (n = 14) mice. In both groups TNFα maximally increased mEPSC frequency within 10 min ($p<0.001$; 2-way repeated measures ANOVA + phc) with comparable effect ($p>0.08$). **E, left**: biocytin staining of the recorded GC showing location of the stimulating electrode and of the puffing pipette containing 60 pM TNFα, accompanied by representative traces (average of 6 consecutive

sweeps) showing paired EPSCs before and 30 min after TNFα puff. Scale bars: 40 ms; 200 pA. **E, middle**: histograms of mean EPSC amplitude and paired-pulse ratio (PPR) in control condition and 30 min after puffing 60 pM TNFα (n = 5; p > 0.27 and p > 0.12, respectively). **E, right**: time-course of the effect of 60 pM TNFα on mean EPSC amplitude (normalized value). **F, left**: GC biocytin staining and corresponding EPSC traces recorded before and after puffing 600 pM TNFα (conditions like in **E, left**). Scale bars: 40 ms; 200 pA. **F, middle**: histograms represent mean eEPSC amplitude and PPR in control condition and 30 min after puffing 600 pM TNFα. The cytokine causes substantial increase of EPSC amplitude (n = 9; p < 0.05) and decrease in PPR (n = 9; p < 0.01); **F, right**: time-course of the effect of 600 pM TNFα on mean EPSC amplitude (normalized value). TNFα induces progressive and irreversible increase in synaptic activity. Data are presented as mean ± SEM. See also Fig. **S1**.

Figure 2: *Mechanism of The Synaptic Change Induced By TNFα: Role of Ifenprodil-Sensitive NMDA Receptors and of TNFR1*. **A, B, C, left:** representative traces of mEPSC frequency in a GC before (control) and 30 min after puffing 600 pM TNFα (different conditions in A, B and C specified below); **right:** time-course of the mean effect of TNFα (normalized value); Scale bars: 5 pA; 5 s. Statistics: repeated measures ANOVA + phc. **A**, TNFα effect in the presence of the NR2B-selective NMDAR antagonist ifenprodil (3 µM, blue bar). The cytokine does not change mEPSC frequency (n = 4, p>0.5 at all time-points after TNFα vs. before TNFα); **B:** TNFα effect when ifenprodil is applied 10 min after puffing the cytokine ($ifenprodil_{post}$). Ifenprodil does not reverse the mEPSC frequency increase induced by TNFα (n = 4; p<0.05: at 5 min post TNFα; p<0.01 at 10 and 20 min; p< 0.001: at 30 min vs. before TNFα); **C:** TNFα effect in *tnfr1*$^{-/-}$ mice. Lack of TNFR1 prevents the effect of TNFα (n = 4; p > 0.4 at all time-points after TNFα vs. before TNFα). Data are presented as mean ± SEM.

Figure 3: *Characterization of hGFAPcreT2/tnfr1$^{cneo/cneo}$ Mice, a Model of Conditional TNFR1 Knock-out in Which TNFR1 Can Be Re-expressed Selectively in Astrocytes.* **A**: scheme of the model: mice expressing TAM-inducible *cre* recombinase under the *hGFAP* promoter (*hGFAPcreT2*) and a conditional reporter (STOP-EYFP, grey triangles) in the *ROSA* locus are crossed with mice (*tnfr1$^{cneo/cneo}$*) with a neomycin cassette (Neo-STOP) flanked by loxP sites inserted in the *tnfr1* gene to conditionally inhibit its functional expression. **B**: representative immunolabeling of the hippocampal DG of a P90 *hGFAPcreT2/tnfr1$^{cneo/cneo}$* mouse upon TAM-induced recombination (z-stack = 12 µm; scale bar = 100 µm). **Upper panels**: **left**: reporter expression revealed by anti-EYFP antibodies (EYFP, red); **middle**: astrocyte staining with glutamine synthetase (GS, green); **right**: overlay showing co-localization of the reporter with astrocytes in the dentate ML and hilus. Notice few additional EYFP^{+} cells in the sub-granular zone (SGZ), representing neural stem cells and/or neuronal precursors. Blue: DAPI nuclear staining. **Lower panels**: **left**: reporter expression as above; **middle**: neuronal staining with NeuN (turquoise); **right**: overlay showing no co-localization of the reporter with neurons. (See also Fig. **S2** for immunolabeling of OIL-treated *hGFAPcreT2/tnfr1$^{cneo/cneo}$* mice). **C**: genomic PCR analysis of *tnfr1* expression in FACS sorted neuronal (NeuN^{+}) and non-neuronal (NeuN^{-}) cell populations from the brains of TAM-injected *hGFAPcreT2/tnfr1$^{cneo/cneo}$*, *tnfr1$^{cneo/cneo}$* and wild-type mice. The lower band (407 bp) corresponds to the wild-type *tnfr1* sequence; the upper one (Unrec, 1836 bp) to the presence of the neo cassette in the *tnfr1* sequence (lack of *tnfr1* expression); the intermediate band (Rec, 576 bp) to the removal of the neo cassette sequence between the 2 loxP sites upon recombination (*tnfr1* re-expression). Note the combined appearance of a strong Rec band and a reduced Unrec band selectively in the NeuN^{-} population from TAM-injected *hGFAPcreT2/tnfr1$^{cneo/cneo}$* mice. See also Fig **S3** and **4**. The β-actin promoter amplicon (bottom) shows the presence of similar amounts of DNA in the reactions. On the left:

molecular weight marker: 100 bp DNA ladder. The gel was cut below 100bp for aesthetic reasons.

Figure 4: *Re-Expression of TNFR1 Selectively in Astrocytes Reconstitutes the Synaptic Effect of TNFα.* **A, B. C left:** representative traces of mEPSC frequency in a GC before (control) and 30 min after puffing 600 pM TNFα (different conditions in A, B and C specified below); **right**: time-course of the mean effect of TNFα (normalized value); Scale bars: 5 pA, 5 s; Statistics: repeated measures ANOVA + phc. **A:** TNFα effect in TAM-injected *hGFAPcreT2/tnfr1*$^{cneo/cneo}$ mice. The cytokine induces persistent increase in mEPSC frequency (n = 7; p<0.01 at all time-points after TNFα vs. before TNFα); **B**: TNFα effect in OIL-injected *hGFAPcreT2/tnfr1*$^{cneo/cneo}$ mice. Without TAM-induced recombination, TNFα does not change mEPSC frequency (n = 3; p >0.3 at all time-points after TNFα vs. before TNFα); **C:** TNFα effect in TAM-injected *tnfr1*$^{cneo/cneo}$ mice. With TAM but without *cre* activity, TNFα does not change mEPSC frequency (n = 5; p > 0.2 at all time-points after TNFα vs. before TNFα. Data are presented as mean ± SEM.

Figure 5: *Impaired Cognitive Function, Local Inflammation and Enhanced TNFα Levels in the Hippocampus of AT-EAE Mice.* **A:** contextual fear learning and memory test in AT-EAE mice (6-7 dpi; blue, n = 7, see also Figs. **S5** and **S6**) vs. vehicle-injected control mice (grey, n = 7); **left:** acquisition of contextual fear conditioning. Mice were first exposed to an activity test (AT) and then to contextual fear conditioning (see also Fig. **S6**). The two groups displayed similar increase in % time spent freezing across intervals (Interval main effect p<0.001 ANOVA + phc) with AT-EAE mice showing slightly lower values; **right:** expression of fear conditioning. AT-EAE mice exhibited decreased freezing (reduced fear memory) compared to control mice (Group x Interval interaction p<0.001 ANOVA + phc) at intervals 1-3, 4-6 and 7-9 (p<0.01; 0.05 and 0.001 respectively). In control mice the level of

freezing at the onset of the expression test was equivalent to that at the end of acquisition. **B:** representative labeling of microglia and leukocyte markers (Iba1, red; CD11b, green) in the hippocampus at the border with the 3rd ventricle (3rd V) in control condition and after AT-EAE induction; blue: DAPI nuclear staining; **left**: large field view (scale bar = 500 µm). Notice in AT-EAE mice (14 dpi) strong accumulation of CD11b-and/or Iba1-positive cells in the 3rd V and surrounding regions (DG and CA3), dissipating towards more distal regions (CA1 and CA2). **Middle**: enlarged views of the DG (ML, GCL) at the border with the 3rd V, corresponding to the dotted squares on the left. The three panels compare the situation in control mice and in AT-EAE mice at 8 and 14 dpi (z-stack = 45 µm; scale bar = 50 µm). An increasing number of infiltrating leukocytes ($CD11b^+$) and activated microglia ($Iba1^+$ and $CD11b^+$) are seen with progression of AT-EAE pathology. **Right**: enlarged views (scale bar = 5 µm) of the white frames in the middle panels highlight the state change of microglia, from resting in control mice (faint Iba1staining) to activated in AT-EAE mice (14 dpi; strong Iba1staining); **C:** TNFα levels in the hippocampus of control (n = 7) and AT-EAE mice (8 dpi; n = 7; same mice as in **A**). Histograms show significant increase in AT-EAE mice compared to controls, specifically in dorsal vs. ventral hippocampus ($p<0.05$; ANOVA + phc). In controls, TNFα values in dorsal and ventral hippocampus were analogous and grouped together. Data are presented as mean ± SEM.

Figure 6: *Altered Hippocampal Excitatory Transmission in AT-EAE: Protective Effect of Ifenprodil.* **A, top**: representative traces of evoked paired-pulse EPSCs in GCs from wild-type vehicle-treated (control, grey) and AT-EAE mice (9 dpi, blue); Scale bars: 40 ms; 200 pA. Stimulation was adjusted to obtain comparable initial EPSC amplitudes in the two groups. Short-term plasticity is altered in AT-EAE mice, leading to reduced paired-pulse facilitation. Histograms show mean PPR in the two conditions (control: n = 10; AT-EAE: n = 8; $p < 0.001$, unpaired t-test); **A, bottom**: mean amplitudes of single EPSCs plotted as function of

the stimulus intensity. EPSCs are larger in GCs from AT-EAE mice than in GCs from control mice (n = 6 and 9, respectively; $p<0.05$, 2-way ANOVA + phc). **B, top**: representative traces of mEPSC activity in dentate GCs from control (n =16) and AT-EAE mice (12 dpi, n = 24). Scale bars: 20 s; 20 pA. The enlarged regions highlight an increased activity in AT-EAE mice. Scale bars: 2 s; 10 pA. **B, bottom**: histograms and representative cumulative probability plots of mean mEPSC frequency (left) and amplitude (right) in control mice and in AT-EAE mice. Both parameters are significantly enhanced in AT-EAE mice ($p<0.001$ and $p<0.05$, respectively, unpaired t-test). **C, top**: representative trace of mEPSC activity in dentate GCs from AT-EAE mice treated with ifenprodil *in vivo* (azure, n = 14). Scale bars: 20 s; 20 pA; the enlarged region shows that activity is lower compared to untreated AT-EAE mice and similar to controls. Scale bars: 2 s; 10 pA. **C, bottom:** histograms showing % change in mean mEPSC frequency (left) and amplitude (right) vs. control in AT-EAE mice treated (azure) or not (blue) with ifenprodil *in vivo*. Untreated but not ifenprodil-treated AT-EAE mice display higher mEPSC frequency than controls ($p<0.001$ and $p = 0.28$, respectively, ANOVA + phc). Concerning mEPSC amplitude, both ifenprodil-treated and untreated AT-EAE mice display higher amplitude than controls ($p<0.05$, ANOVA + phc). Data are presented as mean ± SEM.

Figure 7: *Causal Role of Astrocyte TNFR1 Signaling in the Hippocampal Synaptic Alterations and Cognitive Impairment Induced by AT-EAE.* **A, left**: representative traces of mEPSC activity in dentate GCs upon induction of AT-EAE in mice re-expressing TNFR1 selectively in astrocytes (TAM-treated *hGFAPcreT2/tnfr1*$^{cneo/cneo}$, dark red; n = 21) and in their direct controls (OIL-treated *hGFAPcreT2/tnfr1*$^{cneo/cneo}$, grey; n = 11). Scale bars: 20 s; 20 pA. The enlarged regions highlight higher mEPSC activity in TAM-treated mice compared to OIL-treated ones. Scale bars: 2 s; 10 pA. **A, middle:** histograms showing that mean mEPSC frequency is significantly higher in TAM-treated vs. OIL-treated *hGFAPcreT2/tnfr1*$^{cneo/cneo}$

AT-EAE mice ($p<0.05$, unpaired t-test). **A, right:** representative cumulative probability plots comparing mEPSC IEI in the two above groups. **B**: Histograms showing comparative changes in mEPSC frequency in GCs induced by AT-EAE in several groups of mice with respect to wild-type controls. AT-EAE groups are: wild-type mice (blue, n = 16), TAM- (dark red, n = 21) and OIL-treated (grey, n = 11) *hGFAPcreT2/tnfr1*$^{cneo/cneo}$ mice; TAM- (gold, n = 15) and OIL-treated (green, n = 19) *tnfr1*$^{cneo/cneo}$ mice. AT-EAE causes mEPSC frequency increase only in wild-type and TAM-treated *hGFAPcreT2/tnfr1*$^{cneo/cneo}$ mice ($p < 0.001$ and $p <0.05$ vs wild-type controls, respectively; ANOVA + phc). The latter two groups are not statistically different ($p = 0.095$, ANOVA). **C:** representative labeling of microglia and leukocyte markers (Iba1, red; CD11b, green) in the hippocampal DG of TAM- or OIL-treated *hGFAPcreT2/tnfr1*$^{cneo/cneo}$ (top) and *tnfr1*$^{cneo/cneo}$ (bottom) AT-EAE mice. The pattern of local leukocyte infiltration and microglia activation is similar in the 4 groups of mice and resembles the one observed in wild-type AT-EAE mice (see **Fig. 5B**); z-stack = 20 µm; scale bar: 50 µm. **D**: contextual fear learning and memory test in TAM-treated *hGFAPcreT2/tnfr1*$^{cneo/cneo}$ (dark red, n = 21), OIL-treated *hGFAPcreT2/tnfr1*$^{cneo/cneo}$ (grey, n = 12) and TAM-treated *tnfr1*$^{cneo/cneo}$ mice (gold, n = 11) developing AT-EAE (6-8 dpi). **D, left**: mice were first exposed to an activity test (AT) and then to contextual fear conditioning (see also open field data, Fig. **S7**). For acquisition of fear conditioning, all groups displayed increased % time spent freezing (Interval main effect $p<0.001$, ANOVA + phc). However, TAM-treated *hGFAPcreT2/tnfr1*$^{cneo/cneo}$ mice acquired less fear conditioning than did their OIL-injected counterparts and TAM-treated *tnfr1*$^{cneo/cneo}$ mice (Group x Interval interaction $p<0.003$ ANOVA + phc), whereas the latter two groups were not different; **D, middle**: fear expression test 24h later: there was no difference among the three groups although TAM-treated *hGFAPcreT2/tnfr1*$^{cneo/cneo}$ mice showed a trend to reduced freezing (Group main effect $p=0.06$ ANOVA). **D, right**: repetition of the fear expression test the next day (48h after

conditioning). TAM-treated *hGFAPcreT2/tnfr1*$^{cneo/cneo}$ mice showed a further decrease in freezing and exhibited decreased freezing compared to the other two groups (Group main effect $p<0.002$ ANOVA + phc), whereas OIL-treated *hGFAPcreT2/tnfr1*$^{cneo/cneo}$ mice and TAM-treated *tnfr1*$^{cneo/cneo}$ mice exhibited similar % time freezing. Asterisks are color-coded and refer to comparison with TAM-treated *hGFAPcreT2/tnfr1*$^{cneo/cneo}$ mice. Data are presented as mean ± SEM.

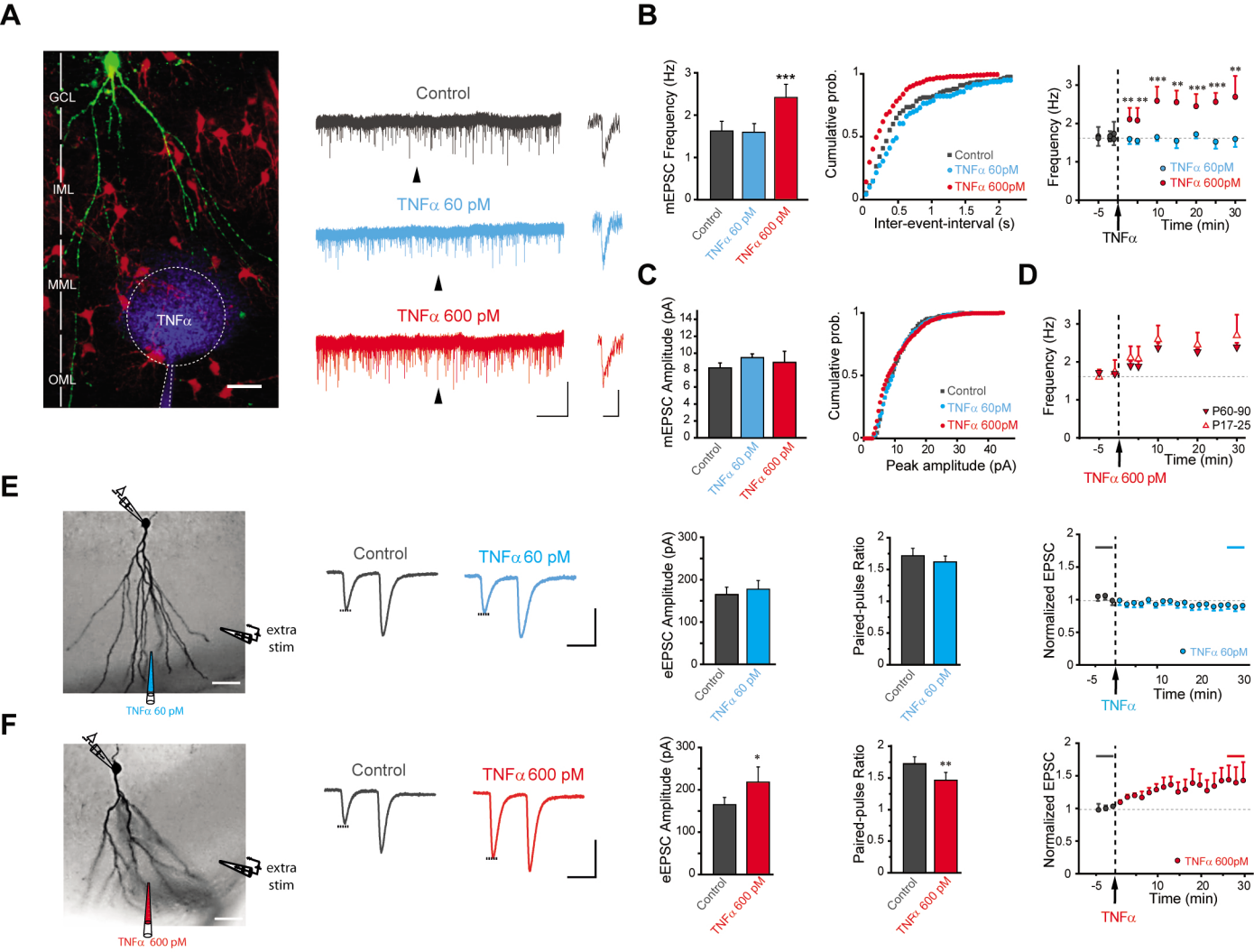

Habbas et al. Fig 1

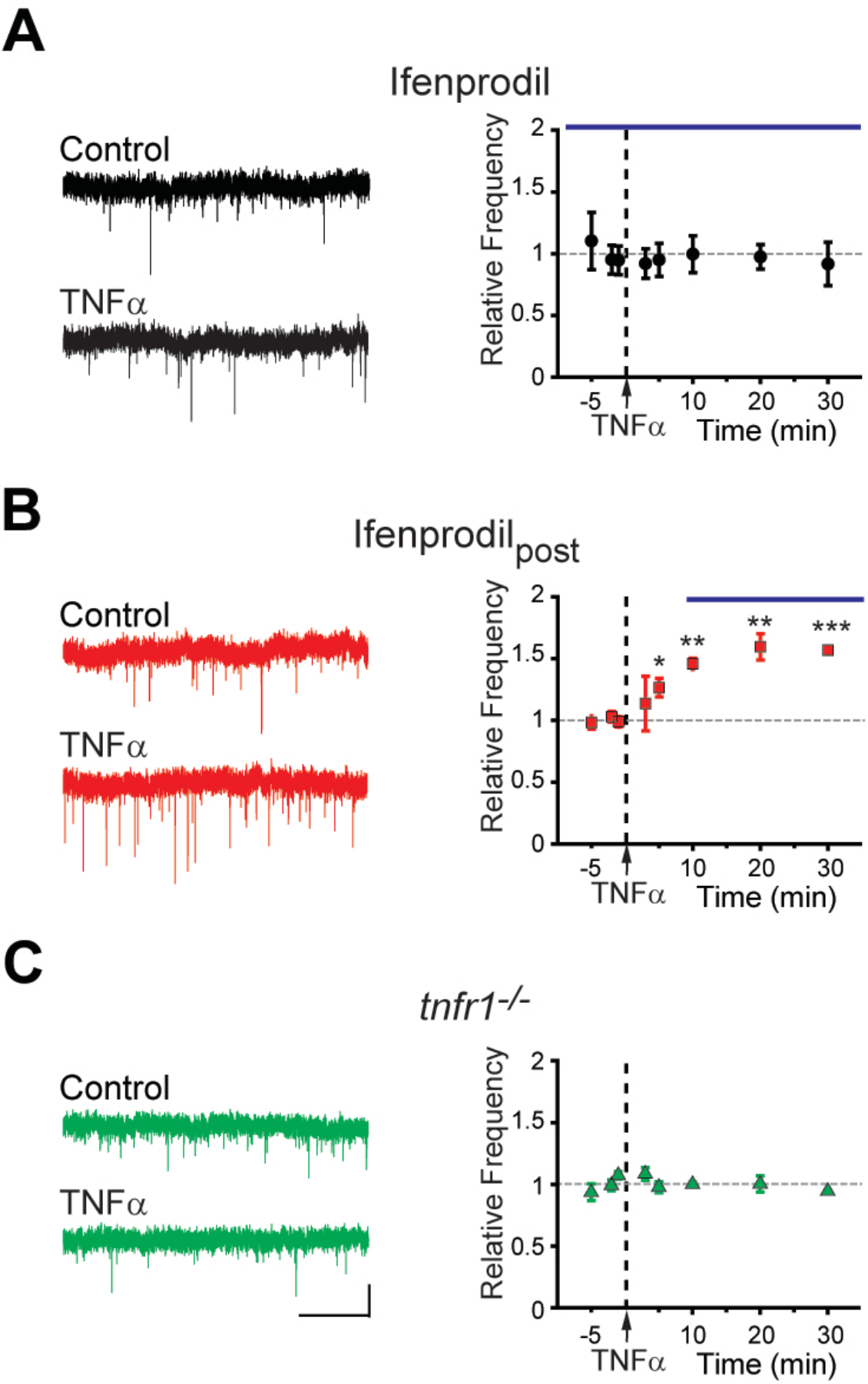

Habbas et al. Fig 2

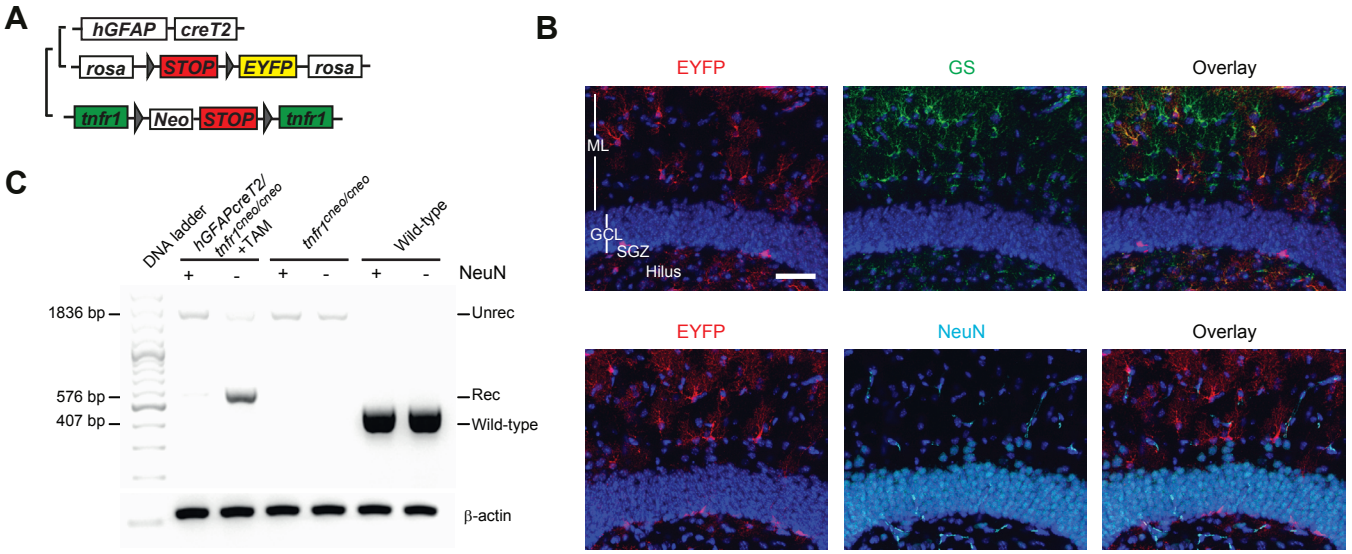

Habbas et al. Fig 3

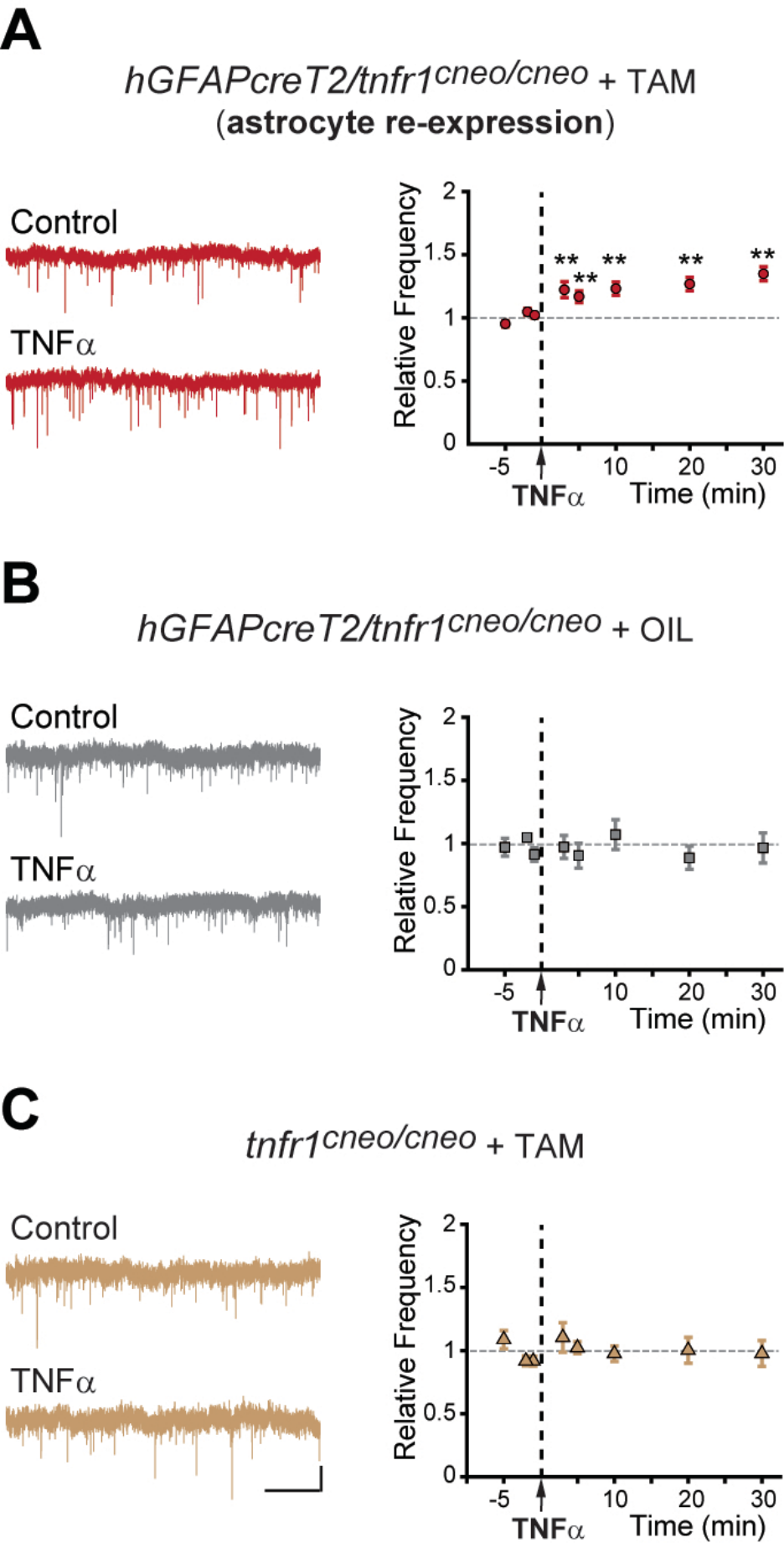

Habbas et al. Fig 4

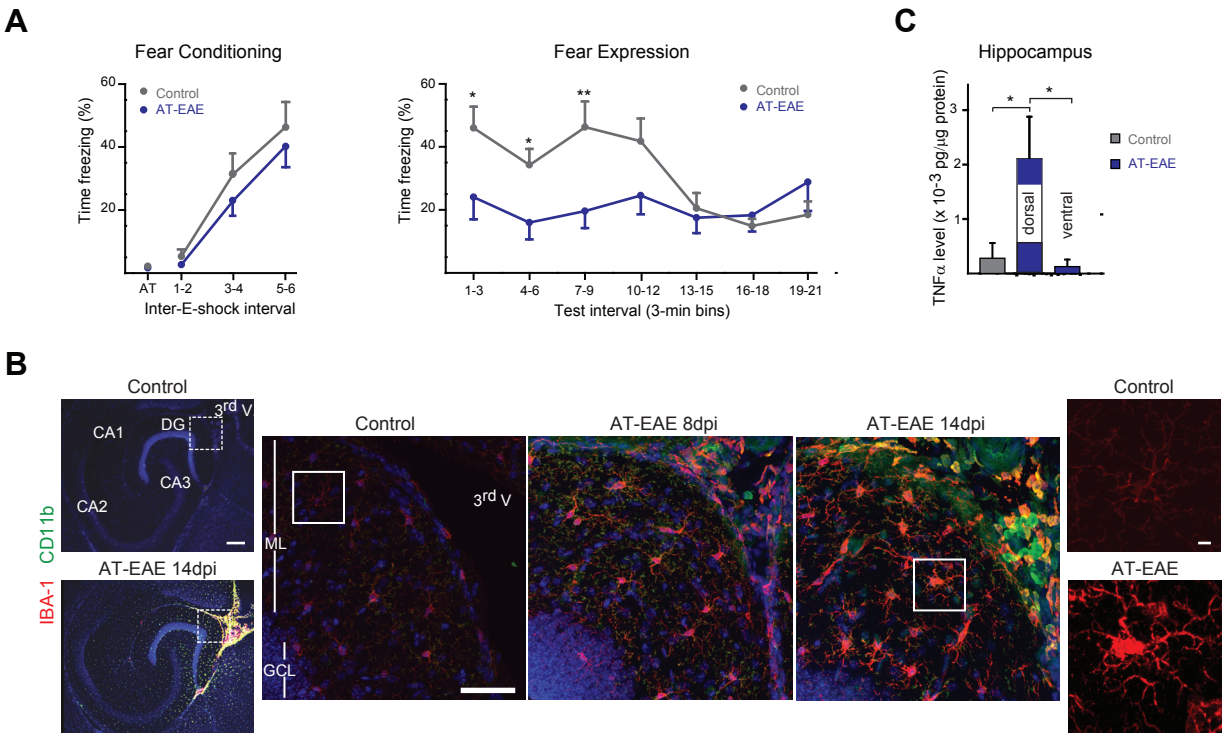

Habbas et al. Fig 5

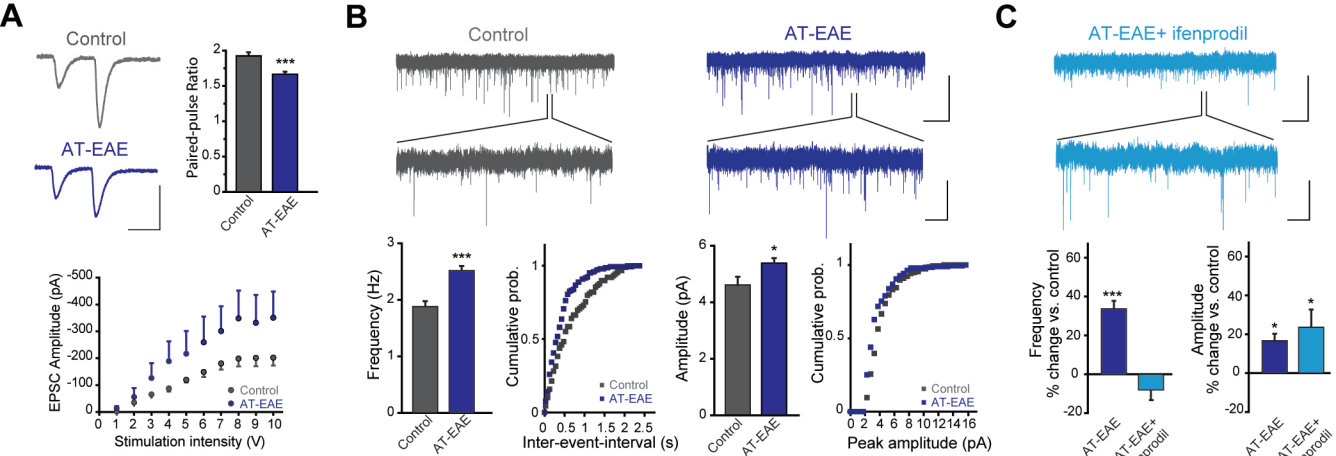

Habbas et al. Fig.6

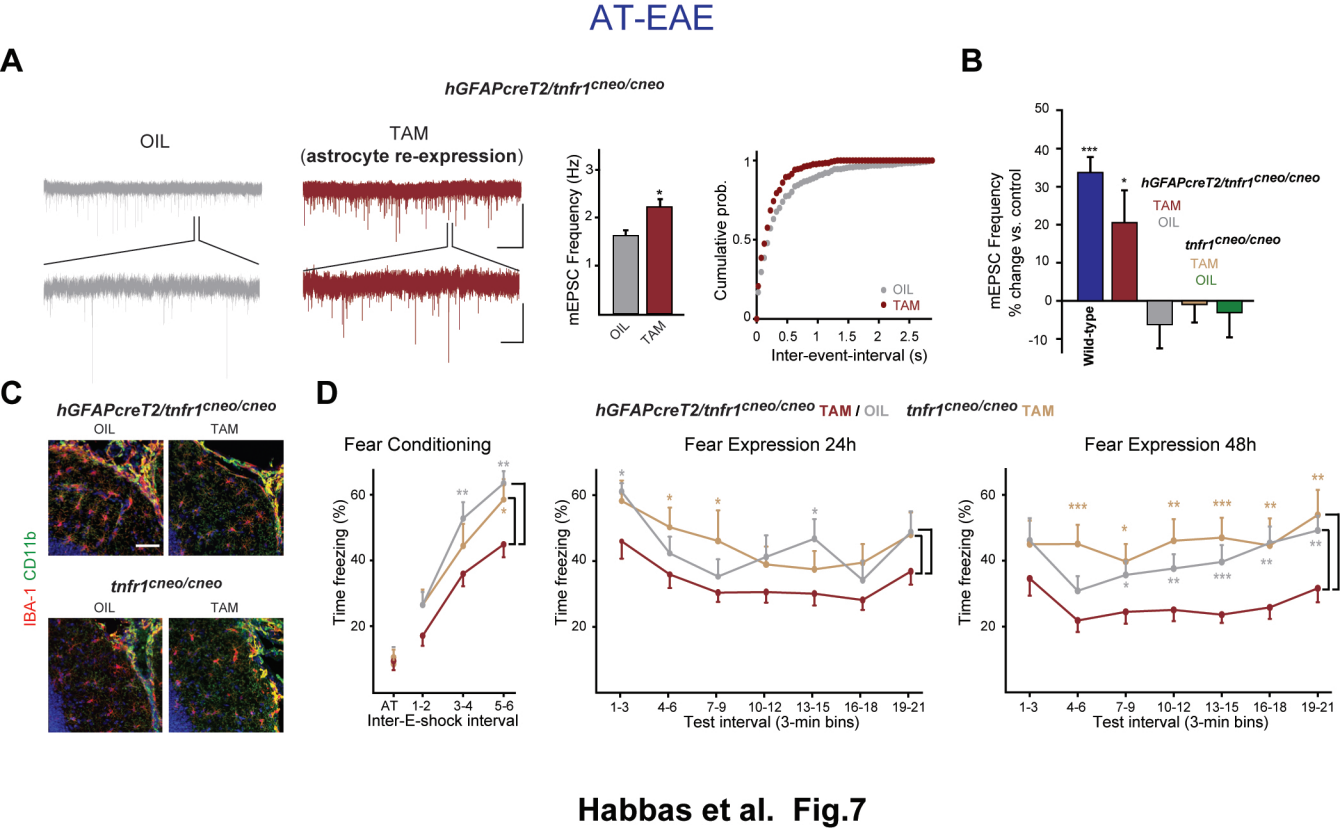

Habbas et al. Fig.7

SUPPLEMENTAL EXPERIMENTAL PROCEDURES

Reagents

Recombinant TNFα and TNFα flow cytometry kit were from R&D System Europe Ltd (Oxon, UK); picrotoxin and ifenprodil from Lucerna-Chem AG; tetrodotoxin from Alomone Labs, Israel; cascade blue, sulforhodamine 101, Alexa Fluor 488, the secondary antibodies Alexa Fluor 555 (rabbit), Alexa Fluor 488 (chicken and rat) and Alexa Fluor 633 (mouse and rabbit) as well as DAPI and ProLong Antifade reagent were from Life Technologies Europe; the primary antibody polyclonal GFP (chicken), which also recognizes EYFP, was from Aves Labs Inc., Oregon, USA (GFP-1010, lot: 0511FP12); polyclonal glutamine synthetase (rabbit) from Abcam, Cambridge, UK (ab73593, lot: GR42622-1); monoclonal NeuN (mouse) from Merck SA, Switzerland (MAB377, lot: 1991263); polyclonal Iba-1 (rabbit) from Wako Chemicals Inc., USA (019-19741, lot: STH6984); monoclonal CD11b (rat) from eBioscience, Inc., San Diego, CA, USA (14-0112, lot: E03532-1630); DMEM and Foetal Bovine Serum were from PAA Laboratories GmbH; papain from Acros Organics, Basel, Switzerland; DNase I from ProSpec, Israel; the genomic DNA purification kit PROMEGA WIZARD AG and the iTaq™ Universal SybrGreen were from Bio-Rad Laboratories AG. All the other chemicals were from Sigma-Aldrich.

Animal models

In our studies we utilized C57BL/6 (wild-type) mice as well as several transgenic lines, some of which were generated within the present study, and all of which were on a C57BL/6 background. *tnfr1*$^{cneo/cneo}$ mice (Victoratos et al., 2006) and *hGFAPcreT2* mice (Hirrlinger et al., 2006) were cross-bred in order to generate *hGFAPcreT2/tnfr1*$^{cneo/cneo}$ mice. All mice were kept in the animal facility according to Swiss guidelines for the welfare of experimental animals. *tnfr1*$^{-/-}$ mice were

housed under specific pathogen-free conditions together with age- and sex-matched wild-type mice. Transgenic lines were screened by PCR analysis for the presence of the transgenes in genomic DNA purified from digital biopsies (5-11 days after birth). The primers used were: for *hGFAPcreT2*: 500 bp, cre-sense 5′- CAG GTT GGA GAG GAG ACG CAT CA-3′ and cre-antisense 5′- CGT TGC ATC GAC CGG TAA TGC AGG C-3′; for *tnfr1*$^{cneo/cneo}$: sense 5-TGG TGG CCT TAA ACC GAT CC-3', antisense: 5'-AGA GAG GTT GCT CAG TGT GAG GC-3', antisense: 5'-ATG ATT GAA CAA GAT GGA TTG CAC-3'; for *ROSA-EYFP*: sense 5'-AAA GTC GCT CTG AGT TGT TAT-3', antisense 5'-GCG AAG AGT TTG TCC TCA ACC-3', antisense 5'-GGA GCG GGA GAA ATG GAT ATG-3', for *tnfr1*$^{-/-}$*:* sense: 5′- GGG GCC TGA GAC CTA ATT GC-3′, antisense 5'-CAG TGA CCC CTG ATG GAT GTA TCC-3′ and antisense 5'-CTT CCA TTT GTC ACG TCC TGC -3′. To achieve gene recombination in living *hGFAPcreT2/tnfr1*$^{cneo/cneo}$ and *tnfr1*$^{cneo/cneo}$ mice the animals were administered TAM dissolved in corn oil (OIL), to a final concentration of 10 mg/ml. Young (P17-25) or adult (P60-90) mice from the same litter were weighted every day and received intra-peritoneal TAM injections (100 mg/kg, one injection/day for 8 consecutive days (Hirrlinger et al., 2006). Some animals received the same injection protocol but with OIL as control carrier. Different intervals from the first TAM/OIL injection were observed in different types of experiment (see main text). Recombination efficacy and specificity were evaluated by genomic PCR analysis (see below) and by EYFP reporter expression (Srinivas et al., 2001) (revealed by GFP immunolabeling, see below). All *in vivo* and *ex vivo* procedures were conducted under license and according to regulations of the Cantonal Veterinary Offices of Vaud and Zurich (Switzerland).

Adoptive-Transfer Experimental Autoimmune Encephalomyelitis (AT-EAE)

The EAE pathology was induced by adoptively transferring via injection effector MOG35–55-specific CD4+ T cells generated from 2D2 mice essentially as described in (Codarri et al. (2011) into P60-90 C57BL/6 (wild-type), *tnfr1*$^{cneo/cneo}$ or *hGFAPcreT2/tnfr1*$^{cneo/cneo}$ mice. The latter two lines from the same litter were treated just before the induction with either TAM or OIL as described above. The adoptive transfer approach was used because the study of EAE was in immune-compromised animals lacking TNFR1 expression in all or most cell types. In order to get around the missing contribution of TNFR1 signaling to the priming phase, that phase was omitted by transferring primed wild-type T cells into the experimental animals. As control, some animals received the same injection protocol but with HBBS buffer only (sham-injected animals). In the days after the encephalitogenic challenge (days post-injection or dpi), mice were monitored, weighed daily, and scored for motor disease severity on a scale of 0 to 5. The score was designated as follows: 0, no detectable signs of EAE; 1, paralysis of the tail; 2, definite tail and partial hind limb paralysis; 3, complete paralysis of the hind limbs; 4, total paralysis of hind and forelimbs (mice at grade 4 were euthanized); 5, moribund or death.

Electrophysiology experiments and analysis

All experiments were executed using C57BL/6 (wild-type) mice or mice from the several transgenic lines detailed above. Depending on the experiment, either young (P17-25) or adult (P60-90) animals were utilized. Some experiments were performed in mice developing AT-EAE, between 8 and 14 dpi. In order to study synaptic function in a cognition-relevant circuit, patch-clamp recordings were performed in acute brain slices maintaining the intact connectivity between entorhinal cortex and hippocampal dentate gyrus. For preparing the acute slices, mice were anesthetized (isoflurane, 1 min) and decapitated. The brain was quickly removed and placed, for

young mice, in ice-cold artificial cerebrospinal fluid (ACSF) containing (in mM) 125 NaCl, 2 KCl, 2 $MgCl_2$, 2 $CaCl_2$, 25 $NaHCO_3$, 1.2 $NaH2PO_4$ and 10 glucose, and for adult mice, in ice-cold sucrose solution containing (in mM) 62.5 NaCl, 105 sucrose, 2 KCl, 7 $MgCl_2$, 0.5 $CaCl_2$, 25 $NaHCO_3$, 1.2 $NaH2PO_4$ and 10 glucose, both at pH 7.4, 295-300 mOsm, saturated with 95% O_2 and 5% CO_2. The brain was then cut (Thermo Scientific Microm International, AG) in horizontal hemibrain slices (350-400 µm-thick) which were allowed to recover in ACSF at 34 °C for at least 45 min before electrophysiological recording. Slices were then transferred individually into a recording chamber where they were submerged and continuously perfused (2 ml/min) with ACSF. All experiments were carried out at 34ºC in the presence of picrotoxin (100 µM), to block $GABA_A$ receptor-mediated inhibitory currents. To study miniature excitatory post-synaptic current (mEPSC) activity in isolation, tetrodotoxin (TTX, 1 µM) was added to the extracellular solution to block action potentials. Recordings were performed at excitatory synapses between perforant path afferents and granule cells (GCs) in the hippocampal dentate gyrus. The latter were patched with borosilicate glass pipettes (3-5 MΩ) containing (in mM): 110 cesium gluconate, 8 NaCl, 0.2 EGTA, 10 HEPES, 17 $CsCl_2$, 0.3 Na_3GTP and 2 Na_2ATP, buffered to pH 7.2–7.4 with CsOH (osmolarity: 290 mOsm). mEPSC recordings were performed with a multiclamp 700B amplifier (DIPSI Industry, France) and acquisitions with pClamp 10.2 (Axon Instruments, Union City, CA), whereas eEPSC recordings were performed using Dagan BVC-700A amplifier (Dagan) and data were acquired with an ITC-16 board (Instrutech) and using Igor software (Wavemetrics). GCs were voltage clamped at –65 mV after reaching whole cell configuration and at least 10 minutes were waited before the beginning of the recording for cell dialysis. Recordings with unstable baseline greater than –200 pA were rejected. TNFα (1 ng/ml (60 pM), or 10 ng/ml (600 pM)) was pressure applied in the dentate molecular layer by using a single 10s pulse. In some experiments the NR2B-selective NMDA receptor antagonist ifenprodil (3 µM) was present. The drug was bath applied

either before or 10 min after TNFα application. To examine the effects of long-term exposure to TNFα, some slices were incubated at room temperature with ACSF containing 60 or 600 pM TNFα for a minimum of 1 hr and a maximum of 2.5 hrs before the experiments started.

In a set of experiments in AT-EAE mice, ifenprodil was administered *in vivo* during induction of the pathology by daily i.p. injection at 40 mg/kg from 5 dpi to the day of the electrophysiological experiment (11-14 dpi). The last injection was performed ≥ 2 h before starting the slicing procedure. Recordings were analyzed as described in Jourdain et al. (2007) and Santello et al. (2011). Transient miniature current events (sampling frequency, 50 kHz) were low-pass filtered (2 kHz) and analyzed in 60 s bins using the Mini-Analysis Program 6.1 (Synaptosoft Inc., USA). In TNFα application experiments, bins were analyzed 5, 2 and 1 minutes before application of the cytokine and 3, 5, 10, 20, and 30 minutes after its application. In some experiments also the 15 and 25 min time points were analyzed. In experiments in which data were expressed as relative frequency, the 3 values of the time points before TNFα application were averaged and considered as the control value. In experiments performed on AT-EAE mice, bins were analyzed ≥10 min after reaching the whole-cell patch-clamp configuration. The selection template chosen to detect each current event consisted of a 5-ms baseline, complete rise time and 90% of decay time. At least 30 events were averaged for any condition in any experiment. Events were identified as miniature excitatory synaptic currents (mEPSC) by setting the event detection threshold at 3-fold the baseline noise level and by checking that events had (i) rise times faster than decay times, (ii) rise times greater than 0.4 ms, and (iii) decay times greater than 1.5 ms. Events not fitting the above parameters were rejected. Event amplitudes, frequencies, rise and decay times were first averaged within each experiment and regrouped by condition. The resulting means were averaged between experiments. Recordings were analyzed with Clampfit 10.2 (Axon Instruments, Union City, CA). For all graphs Origin 8.1 (OriginLab Corporation, Northampton, MA) was used. eEPSCs were

evoked by placing a theta patch pipette located in the outer molecular layer 50-100 µM lateral from the recorded GC. Synapses were stimulated every 20 s with a 20-Hz paired-pulse. Stimulation intensity was adjusted in order to obtain current amplitude of 100-200 pA and a stable baseline for at least 5 min. Recordings with leak increasing more than 100 pA, access resistance changing more than 20% or EPSC amplitude rundown more than 10% between the beginning and the end of the baseline period were discarded. Six consecutive sweeps immediately before TNFα puff and at the end of the time-course were averaged to evaluate changes in EPSC amplitude and paired-pulse ratio (PPR). For experiments on AT-EAE mice, a single EPSC was evoked every 10 s at increasing stimulation intensities whereas 5 paired-pulses (every 20 s) were recorded at adjusted stimulation intensity and averaged between them to obtain the PPR. Whenever possible, neurons directly facing the 3rd ventricle were recorded. Some cells were filled with 0.2% biocytin to reveal their morphology detail and PFA-fixed slices were developed with the avidin-biotin-peroxidase method (Egger et al., 2008).

Two-Photon imaging

Two-photon imaging was performed with an Ultima two-photon laser scanning microscope (Brucker Nano Surfaces Division, Madison, WI, USA), consisting of an Olympus BX61WI with a Bruker galvanometer scanning system and a 60× water immersion objective lens (numerical aperture: 0.9; Olympus Optical LUMPlan FI/IR). To reveal astrocytes, these cells were live stained with the red dye sulforhodamine 101 (0.1 µM; 15 min, 37°C), whereas the fine morphology of patched GCs was revealed by adding the green dye Alexa 488 (200 µM) to the intracellular patch solution and by letting the dye diffuse into the cell (30 min) after reaching the whole-cell configuration. Application of TNFα-containing solution (see above) was monitored with the dye

Cascade blue (500 μM) added to the solution. Simultaneous acquisition (wavelength: 820 nm; frame rate: 0.5 Hz; dwell time: 0.8 μs; resolution: 1024x1024) of red, green and blue fluorescence and of high-contrast transmitted-light (via Dodt contrast) before, during and after the TNFα pulse was used to establish the position of the ejection pipette relative to the recorded GC and neighboring astrocytes, and to monitor the spatial domain of diffusion and the subsequent rapid washout of the TNFα-containing solution following pulse application.

Immunohistochemistry and image analysis

Immunohistochemistry (IHC) experiments were performed in slice preparations from: (a) *hGFAPcreT2/tnfr1*$^{cneo/cneo}$ mice injected with either TAM or OIL to evaluate cell-specific reconstitution of gene expression; and (b) C57BL/6 (wild-type) mice and different transgenic lines (*tnfr1*$^{cneo/cneo}$, *hGFAPcreT2/tnfr1*$^{cneo/cneo}$ mice injected with either TAM or OIL) to evaluate progression of local inflammation upon AT-EAE induction. Image analysis was performed in the hippocampal dentate gyrus. In the local inflammation experiments the whole hippocampal formation and the other regions surrounding the 3rd ventricle were considered. In all cases, mice were anesthetized with isoflurane and decapitated. Brains were fixed overnight (4% paraformaldehyde in PBS) at 4°C, washed 4 times in PBS and incubated for 1.5 days in 30% fresh sucrose in PBS at 4° C. 50 μm-thick horizontal brain slices were cut with a cryo-microtome (Microm International AG) and stored at -20° C in a solution containing ethylene glycol (30%) and glycerol (30%) in 0.05 M phosphate buffer (PB, pH 7.4) until further processing. For IHC, slices rinsed in PBS (3 x 10 min), were permeabilized with 0.3% Triton-X 100 (10 min), incubated with blocking solution (0.3% Triton-X 100, 2% horse serum in PBS, 2 h) and with primary antibodies on a horizontal shaker (72 h, 4°C), then washed in PBS (3 x 10 min) and incubated with secondary

antibodies in 0.3% triton-X 100/PBS at room temperature for 2 h. Next, slices were washed (2 x 10 min) in 0.1 M PB (pH 7.4) and incubated with 4′,6-diamidino-2-phenylindole (DAPI, 300 nM) to label nuclei, washed again in 0.1 M PB (pH 7.4) and mounted on glass slides using ProLong Gold Antifade reagent for analysis with confocal microscopy. In experiments looking at gene re-expression, slices were incubated with anti-GFP (1:1000), which also recognizes EYFP, anti-glutamine synthetase (1:500) or anti-NeuN (1:500) antibodies revealed with anti-chicken Alexa Fluor 488 (1:400), anti-rabbit Alexa Fluor 633 (1:400) and anti-mouse Alexa Fluor 633 (1:400), respectively. In experiments looking at progression of local inflammation, slices were incubated with anti Iba-1 (1:400) and anti-CD11b (1:250) antibodies revealed with anti-rabbit Alexa Fluor 555 (1:400) and anti-rat Alexa Fluor 488 (1:400), respectively. A Leica MZ16FA stereomicroscope (Leica Microsystems, Germany) equipped with Leica EL6000 illumination was used for large filed images whereas a Leica SP5 AOBS confocal microscope (Leica Microsystems, Germany) and using a 40x oil immersion objective (NA: 1.25-0.75) was used in all other cases. For each fluorophore, acquisition consisted of a z-stack (12-45 µm; step size: 0.3-1 µm, frame average: 2, scan speed: 400 Hz, pinhole size: 1 Airy unit; resolution: 1024 x 1024 or 512 x 512 pixels). Laser excitation wavelength was set at: 405 nm with a diode through an acousto-optic beam splitter for DAPI; 488 nm with Argon laser for Alexa Fluor 488; 543 nm and 633 nm with a He/Ne laser for Alexa Fluor 555 and Alexa Fluor 633, respectively. Images were visualized with Imaris software (Bitplane AG, Zurich, Switzerland), transformed into tiff grayscale images for each channel and analyzed with ImageJ software (NIH, USA). To assess recombination efficacy, cells expressing the reporter gene (EYFP-positive cells) were counted in the whole dentate gyrus region with “easy 3D function” and expressed as % of GS-positive cells or NeuN-positive cells. In all cases, 3 slices from 4 animals/group were analyzed. Images in the figures are maximal intensity projections with median filter and contrast adjusted for display purposes.

Flow cytometric sorting and genomic PCR analysis of brain cell populations

The protocol used for purification of different brain cell populations was essentially as described in Lioy et al. (2011). Briefly, whole brains from adult C57BL/6 (wild-type) , *tnfr1*$^{cneo/cneo}$ or TAM-injected *hGFAPcreT2/tnfr1*$^{cneo/cneo}$ mice were cut quickly into small pieces in cold dissociation medium and incubated (45 min, 37°C) in the same medium containing 40 U/ml papain. The resulting tissue was washed, mechanically triturated in DMEM containing 0.5 mg/ml DNase-I and 10% fetal bovine serum (FBS) and consecutively filtered with 100 µm and 40 µm strainers to separate intact cells from cell debris or aggregates. After centrifugation (10 min, 1000 rpm 4ºC), cells were fixed with 1% formaldehyde (15 min, 25ºC), washed twice in DPBS then permeabilized in PBS containing 0.2% TritonX-100 and 10% FBS (30 min, 25ºC). Cells were labeled using anti-mouse NeuN antibody (1:200) followed by anti-mouse Alexa Fluor 488 (1:300, 1h at room temperature); nuclei were labeled with DAPI (300 nM). The different cell populations were discriminated by flow cytometric sorting (BD FACS Aria I, BD Biosciences, Switzerland, Europe) analysis (Guez-Barber et al., 2012). DAPI-labelled cells were separated in neuronal ($NeuN^+$) and non-neuronal ($NeuN^-$) cells according to positive or negative NeuN labeling. Sorting parameters were adjusted to achieve the optimal purity for each group. Validations of the sorting parameters and of the sample purity were done by reanalyzing the sorted cells. Data were analyzed with FlowJo software (Tree Star, Ashland, OR, USA). After sorting, DNA was quickly extracted from $NeuN^+$ and $NeuN^-$ cell populations using a genomic DNA purification kit. PCR and semi-quantitative PCR experiments were done using iTaq™ Universal SybrGreen® and the following *tnfr1* primer sequences: sense: 5'-GG TGG CCT TAA ACC GAT CC-3'; antisense: 5'-AGA GAG GTT GCT CAG TGT GAG GC-3'. Quantification of the different bands was made with ImageJ software by

manually drawing a region of interest (ROI) corresponding to the area of the smallest defined band and quantifying the fluorescence intensity within the ROI after background subtraction. β-actin was used as a control of the quantity of DNA loaded for the different cell populations. The following primers were used: sense 5'- CCC AAC ACA CCT AGC AAA TTA GAA CCA C-3' and antisense 5'-CCT GGA TTG AAT GGA CAG AGA GTC ACT-3'.

Behavioural experiments

Behavioural testing for acquisition of contextual fear conditioning in adult C57BL/6 (wild-type) mice developing AT-EAE (6 and 7 dpi) and sham-injected controls was conducted using a Multi Conditioning System (TSE Systems GmbH, Bad-Homburg, Germany), details of which are given in Pryce et al. (2012). Behavioural testing in adult *hGFAPcreT2/tnfr1*$^{cneo/cneo}$ mice, their *tnfr1*$^{cneo/cneo}$ littermates (TAM- or OIL-treated as indicated in the figures), and also wild-type mice, developing AT-EAE (6-8 dpi, max. 16 days after the first TAM injection), was carried out using a fear conditioning arena placed within an isolation chamber (Ugo Basile, Italy) controlled by Ethovision XT software (Noldus, Netherlands). In all experiments, mice were placed in an arena (context) with a grid floor which could be electrified. A first 5-min activity test (AT) in the absence of electro-shocks was followed by the conditioning session, comprising six inescapable electro-shocks each of 0.20 mA x 2 s, delivered at intervals of 2 min. On the following day (24 h test) and in some experiments also the next day (48 h test), mice were placed back in the same arena in the absence of electro-shocks for the mnemonic fear expression test comprising 21 min divided into 1 min intervals. The main measure in each test was the % time spent freezing per interval, with freezing defined as an episode during which no movement was detected for at least 2 s. For conditioning, mean % time freezing was calculated for each pair of consecutive intervals between

electro-shocks (1-2, 3-4, 5-6); for the expression test mean % time freezing was calculated for each trio of consecutive intervals (1-3, 4-6, 7-9, 10-12, 13-15, 16-18, 19-21). In addition, the measure of distance moved during the electroshock delivery was utilized as an indicator of pain sensitivity, i.e. distance moved is assumed to be proportional to pain sensitivity.

In the transgenic mice, an open-field test was conducted on animals developing AT-EAE (5 dpi) the day before investigation of the same animals in contextual fear conditioning (see above). The open-field test was then repeated at 9dpi, after the last fear expression test. The square open-field arena was 45 x 45 x 40 (H) cm and made of grey plastic. Illumination was set at 70-80 lux. Mice were gently placed in the middle of the open field and allowed to freely explore the arena for 20 min. The mice were continuously recorded using a video camera placed above the arena and the images were analyzed using Ethovision XT software (Noldus, Netherland). Mean speed, total distance travelled and time spent immobile were measured to assess locomotor activity and exploration. The time spent in a virtual inner zone (15 x 15 cm area in the middle of the arena) was measured as an inverse index of anxiety. All behavioural apparatus was carefully washed with 70% ethanol solution in between tests.

Measure of TNFα tissue concentration

Brains from C57BL/6J AT-EAE and sham-injected control mice previously subjected to behavioural testing (see above) were rapidly extracted and frozen at -80°C. For each brain, 1000 µm coronal sections were prepared at -18 °C using a brain matrix (Azzinnari et al., 2014). Each section containing the hippocampus was then micropunched (punch size: 0.5 or 1 mm depending on the section) to obtain tissue samples containing specifically either the dorsal or the ventral part of the hippocampus. Samples were individually weighted, dissolved in ice-cold complete Tris lysis

buffer (Meso Scale Discovery, Rockville, MD, USA) and homogenized using an ultrasonicator. After centrifugation (14.000 rpm, 10 min), the supernatants were collected. 10 µl of each supernatant were used for total protein quantification (Coomassie Plus (Bradford) Assay Kit, Thermo Fisher Scientific Inc., Waltham, MA, USA); the remaining 90 µl were used for determination of the TNFα concentration using a multiplexed particle-based flow cytometric cytokine assay (Azzinnari et al., 2014; Vignali, 2000). Each sample was measured in duplicate and the mean was normalized to the protein content of the sample and expressed as pg/µg protein.

Statistical analysis

Unpaired t-tests were used when comparing the means of two independent experimental populations. In cases where the populations were not independent, e.g. when synaptic activity was compared at two time points before and after TNFα application, paired t-tests were used. ANOVA was used when comparing the means of more than two populations. Repeated measures ANOVA with or without independent treatment groups was performed on time-course experiments, e.g. synaptic activity at different time points before and after TNFα application, or AT-EAE vs. control mice in fear-freezing behaviour. In cases where ANOVA tests yielded significant effects, appropriate post hoc comparisons were used to identify significant pairwise differences. Two-way ANOVA was used to compare stimulus-EPSC amplitude profile between control and AT-EAE groups. For statistical analyses jmp10, GraphPad Prism 6 (GraphPad software, USA) and Excel were used. Values are expressed as mean ± s.e.m. unless otherwise specified. Data were considered as significantly different when the p value was less than 0.05. p values less than 0.05, 0.01 and 0.001 were indicated with (*), (**) and (***) respectively.

REFERENCES

Azzinnari, D, Sigrist, H, Staehli, S, Palme, R, Hildebrandt, T, Leparc, G, Hengerer, B, Seifritz, E, and Pryce, CR (2014). Mouse social stress induces increased fear conditioning, helplessness and fatigue to physical challenge together with markers of altered immune and dopamine function. Neuropharmacology *85*, 328-341.

Codarri, L, Gyulveszi, G, Tosevski, V, Hesske, L, Fontana, A, Magnenat, L, Suter, T, and Becher, B (2011). RORgammat drives production of the cytokine GM-CSF in helper T cells, which is essential for the effector phase of autoimmune neuroinflammation. Nat Immunol *12*, 560-567.

Egger, V, Nevian, T, and Bruno, RM (2008). Subcolumnar dendritic and axonal organization of spiny stellate and star pyramid neurons within a barrel in rat somatosensory cortex. Cereb Cortex *18*, 876-889.

Guez-Barber, D, Fanous, S, Harvey, BK, Zhang, Y, Lehrmann, E, Becker, KG, Picciotto, MR, and Hope, BT (2012). FACS purification of immunolabeled cell types from adult rat brain. J Neurosci Methods *203*, 10-18.

Hirrlinger, PG, Scheller, A, Braun, C, Hirrlinger, J, and Kirchhoff, F (2006). Temporal control of gene recombination in astrocytes by transgenic expression of the tamoxifen-inducible DNA recombinase variant CreERT2. Glia *54*, 11-20.

Jourdain, P, Bergersen, LH, Bhaukaurally, K, Bezzi, P, Santello, M, Domercq, M, Matute, C, Tonello, F, Gundersen, V, and Volterra, A (2007). Glutamate exocytosis from astrocytes controls synaptic strength. Nat Neurosci *10*, 331-339.

Lioy, DT, Garg, SK, Monaghan, CE, Raber, J, Foust, KD, Kaspar, BK, Hirrlinger, PG, Kirchhoff, F, Bissonnette, JM *et al.* (2011). A role for glia in the progression of Rett's syndrome. Nature *475*, 497-500.

Pryce, CR, Azzinnari, D, Sigrist, H, Gschwind, T, Lesch, KP, and Seifritz, E (2012). Establishing a learned-helplessness effect paradigm in C57BL/6 mice: behavioural evidence for emotional, motivational and cognitive effects of aversive uncontrollability per se. Neuropharmacology *62*, 358-372.

Santello, M, Bezzi, P, and Volterra, A (2011). TNFalpha controls glutamatergic gliotransmission in the hippocampal dentate gyrus. Neuron *69*, 988-1001.

Srinivas, S, Watanabe, T, Lin, CS, William, CM, Tanabe, Y, Jessell, TM, and Costantini, F (2001). Cre reporter strains produced by targeted insertion of EYFP and ECFP into the ROSA26 locus. BMC Dev Biol *1*, 4.

Victoratos, P, Lagnel, J, Tzima, S, Alimzhanov, MB, Rajewsky, K, Pasparakis, M, and Kollias, G (2006). FDC-specific functions of p55TNFR and IKK2 in the development of FDC networks and of antibody responses. Immunity *24*, 65-77.

Vignali, DA (2000). Multiplexed particle-based flow cytometric assays. J Immunol Methods *243*, 243-255.

Figure S1 (related to Figure 1): *Rapid Application of Exogenous TNFα (60 or 600 pM) Does Not Affect mEPSC Amplitude and Kinetics in a Hippocampal Cognitive Circuit, Whereas Prolonged Incubation of the Cytokine (600 pM) Affects Both mEPSC Frequency and Amplitude.*

A: Time-course of mean values of mEPSC amplitude (**left**), rise time (**middle**) and decay time (**right**) in the period going from 5 min before application of TNFα (60 pM: blue; 600 pM: red) up to 30 min after application of the cytokine. No difference was observed in any of the three parameters at any time, before or after TNFα application, with the low or the high cytokine concentration (amplitude: $p>0.2$; rise time: $p>0.2$; decay time: $p>0.06$ for all time points, repeated measures ANOVA). **B:** histograms of mean mEPSC frequency, amplitude, rise time and decay time (from left to right) after 1-2.5 h incubation of 600 pM TNFα (n=13) compared to control condition (n=16). Note that, with this protocol, not only mEPSC frequency ($p<0.001$, unpaired t-test) but also mEPSC amplitude ($p<0.05$, unpaired t-test) was significantly increased by TNFα above the value in control condition. In contrast, no effect was observed on rise time ($p>0.09$, unpaired t-test) or decay time ($p>0.19$, unpaired t-test), like upon short puff of the cytokine. Data are presented as mean ± SEM.

Figure S2 (related to Figure 3): *Lack of Reporter Expression in OIL-treated hGFAPcreT2/tnfr1$^{cneo/cneo}$ Mice.* Representative immunolabeling of the hippocampal dentate gyrus of a 90-days old *hGFAPcreT2/tnfr1$^{cneo/cneo}$* mouse injected with OIL (z-stack = 12 µm; scale bar = 100 µm). **Upper panels:** dual labeling with anti-EYFP antibodies (left, EYFP) and the astrocyte specific marker glutamine synthetase (right, GS, green) shows no reporter expression in astrocytes, indicative of lack of recombination in these cells. **Lower panels:** dual labeling with EYFP and the neuronal specific marker NeuN (turquoise) excludes reporter expression also in neurons. Blue corresponds to DAPI nuclear staining.

Figure S3 (related to Figure 3): *Separation of Neurons and Non-neuronal Cells From the Brains of Different Mouse Groups Via Flow Cytometric Sorting.* Flow cytometric analysis was performed on cells enzymatically dissociated from adult mouse brains and fluorescently labeled with DAPI and Alexa Fluor 488 directed against the neuronal marker NeuN (Alexa Fluor 488-A, see Methods). The following mouse groups were analyzed: **A:** wild-type (n = 12 mice); **B:** TAM-treated *hGFAPcreT2/tnfr1*$^{cneo/cneo}$ (n = 8); **C:** *tnfr1*$^{cneo/cneo}$ (n = 7). For each mouse group, cells were separated in neuronal and non-neuronal populations according to the presence ($NeuN^+$, purple) or absence ($NeuN^-$, orange) of Alexa Fluor 488-A fluorescence. In order to distinguish single cells from cell clusters, singlet gating based on a DAPI-A vs DAPI-W scatter plot was done (Guez-Barber et al., 2012). $NeuN^+$ and $NeuN^-$ singlets were then sorted. Singlets presented the following % of fluorescent events/population: for wild-type mice: $NeuN^+$: 88.7; $NeuN^-$: 89.2; for TAM-treated *hGFAPcreT2/tnfr1*$^{cneo/cneo}$ mice: $NeuN^+$: 86.2; $NeuN^-$: 46.1; for *tnfr1*$^{cneo/cneo}$ mice: $NeuN^+$: 74.6; $NeuN^-$: 64.9. **Right panels:** graphs showing the sorted $NeuN^+$ and $NeuN^-$ singlet populations. Horizontal bars indicate the proportion of cells in each sorted population that were subsequently used for genomic PCR analysis (Fig. 3c), namely: 40.7% of $NeuN^+$ and 84.9% of $NeuN^-$ cells from wild-type mice; 57.4% of $NeuN^+$ and 68.6% of $NeuN^-$ cells from TAM-treated *hGFAPcreT2/tnfr1*$^{cneo/cneo}$ mice; 65.2% of $NeuN^+$ and 94.6% of $NeuN^-$ cells for *tnfr1*$^{cneo/cneo}$ mice. Note that, although we selected the above proportions restrictively, we cannot exclude small contaminations.

Figure S4 (related to Figure 3): *Semi-quantitative Genomic PCR Analysis of tnfr1 Expression in NeuN^{+} and NeuN^{-} Cell Populations From the Brains of TAM-treated hGFAPcreT2/tnfr1$^{cneo/cneo}$ Mice.* **Left, top**: PCR gel pictures corresponding to the bands of unrecombined (Unrec, grey) and recombined (Rec, dark red) DNA after 24, 25, 26 and 27 PCR cycles in the NeuN^{+} cell population. The Rec band reflects the amount of *tnfr1* specific re-expression. **Left, bottom:** bar-graph reporting the intensity of each band after each given number of PCR cycles. While the intensity of the Unrec band increases with the PCR cycles, no Rec band was detected in this population even after 27 cycles. **Middle, top and bottom:** same experiment as above but performed using the NeuN^{-} cell population. Note in this case that the Rec band is present already after 24 PCR cycles and that the Unrec band reaches plateau already after 26 cycles. **Right:** same experiment as above but performed using β-actin primers to test the relative amplification of β-actin in the NeuN^{+} (purple) and NeuN^{-} (orange) cell populations as control. As expected, similar DNA copy numbers are observed in the two populations.

Figure S5 (related to Figure 5): *Course of AT-EAE Development And Underlying Motor Dysfunction in Wild-type Mice.* The graph gives the incidence of AT-EAE (blue) and underlying daily mean motor disease severity scores (red) (n = 16 mice in 3 experimental series). Daily assessments were made during the first 15 days following adoptive transfer of 2D2 transgenic CD4 T cells primed in vivo and re-stimulated in vitro. Motor disease severity was scored from 0 to 5 (see Methods). Data are presented as mean ± SEM.

Figure S6 (related to Figure 5): *Measures of Locomotor Activity, Anxiety, Exploratory Activity and Pain Sensitivity Show No Difference Between AT-EAE Mice and Controls.* Histograms of the different behaviors measured in wild-type mice developing AT-EAE at 6 dpi (AT-EAE, blue bars, n = 7) and in their sham-treated controls (Control, grey bars, n = 7). Measures were taken during a 5-min activity test preceding the fear conditioning test or during the fear conditioning test itself. From left to right, total distance travelled (index of locomotor activity), percentage of time spent freezing (index of anxiety) and total incidence of rearing (index of exploratory activity) were assessed during the activity test. No significant difference was observed between AT-EAE and control mice ($p > 0.56$, unpaired t-test). Mean total distance moved during the 6 x 2-sec electroshocks in the fear conditioning test was measured as an index of pain sensitivity, no significant difference was observed ($p = 0.83$, unpaired t-test). Data are presented as mean ± SEM.

Figure S7 (related to Fig. 7): *Measures of Locomotor Activity, Anxiety, Exploratory Activity and Pain Sensitivity Show No Difference Between Three Groups of AT-EAE Mice: TAM-Treated And OIL-treated hGFAPcreT2/tnfr1$^{cneo/cneo}$ Mice And TAM-treated tnfr1$^{cneo/cneo}$ Mice.* **A:** example traces of locomotor activity in OIL (grey, n = 12), TAM-treated (dark red, n = 21) *hGFAPcreT2/tnfr1$^{cneo/cneo}$* mice, and in TAM-treated *tnfr1$^{cneo/cneo}$* mice (gold, n = 11) placed in an open field for 20 min at 5 dpi of AT-EAE. Scale bar: 5 cm. **B**: histograms of the total distance travelled (index of locomotor activity), speed (index of locomotor activity), time spent immobile (index of inactivity) and time spent in the inner zone (inverse index of anxiety) by the mice during the open field test show no significant differences between the 3 groups ($p > 0.58$ ANOVA). **C, left**: histograms of total number of rearings during the 5 min activity test (index of exploratory activity). **C, right**: mean of the total distance moved during the 6 x 2-sec electro-shocks in the fear conditioning test (index of pain sensitivity). No difference was found between the 3 mouse groups for the 2 above parameters ($p > 0.26$ ANOVA). Data are presented as mean ± SEM.

Supplemental Figure 1

Click here to download Supplemental Figure SupplFig1.pdf

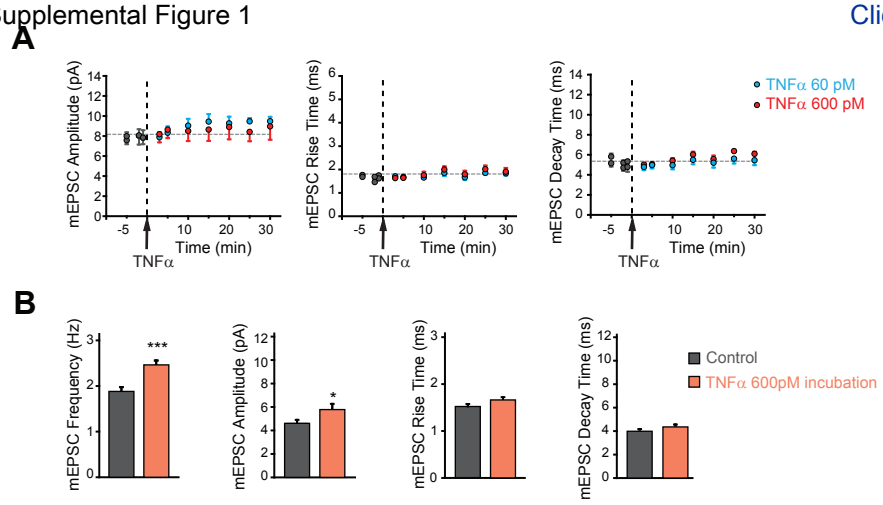

Figure S1 Related to Figure 1

Supplemental Figure 2

Click here to download Supplemental Figure SupplFig2.pdf

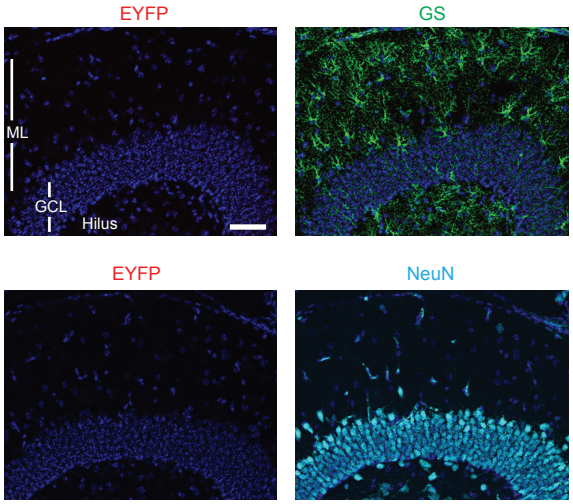

Figure S2 Related to Figure 3

Click here to download Supplemental Figure supplFig3.pdf

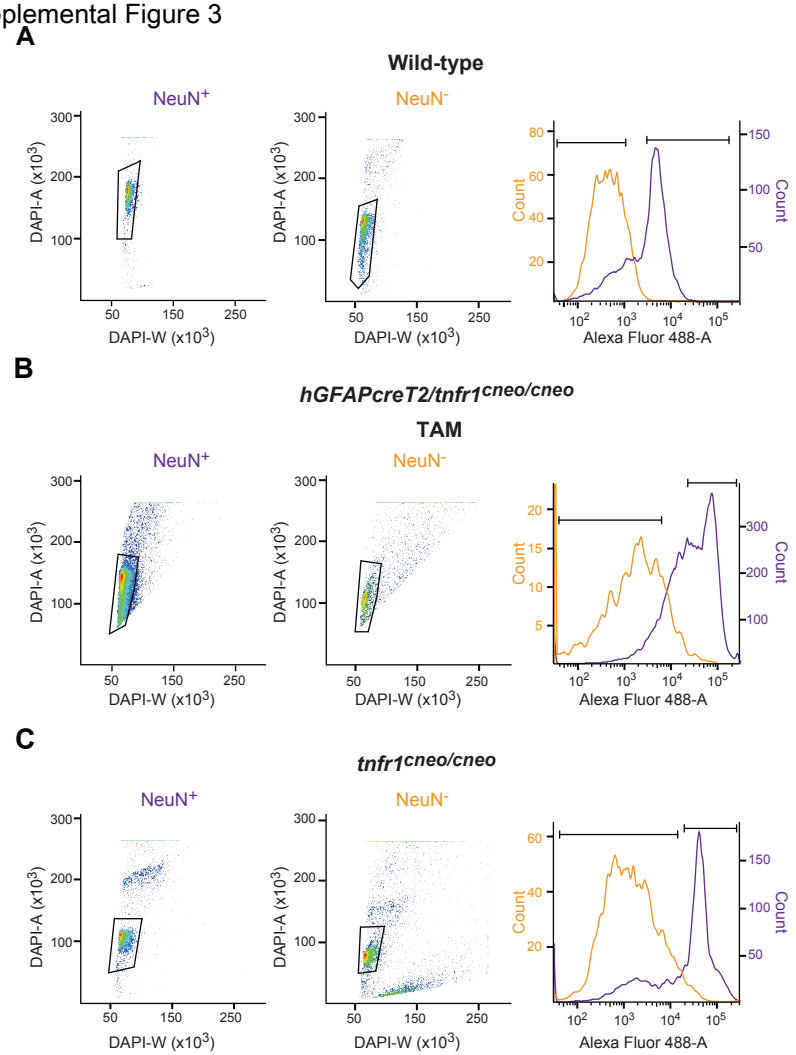

Figure S3 Related to Figure 3

Supplemental Figure 4

Click here to download Supplemental Figure SupplFig4.pdf

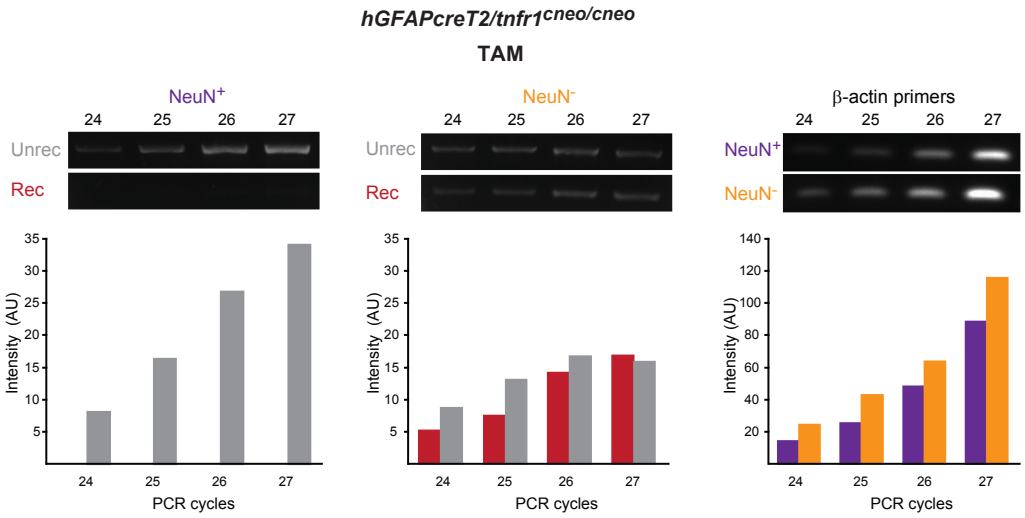

Figure S4 Related to Figure 3

Supplemental Figure 5

Click here to download Supplemental Figure SupplFig5.pdf

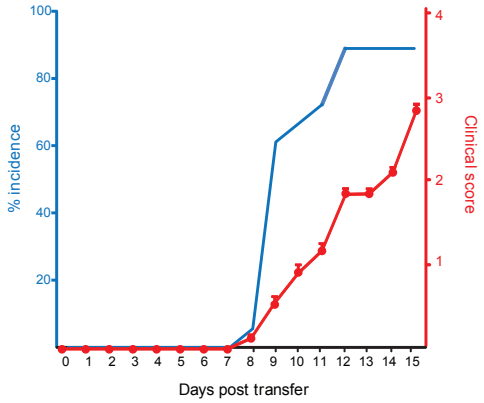

Figure S5 Related to Figure 5

Click here to download Supplemental Figure SupplFig6.pdf

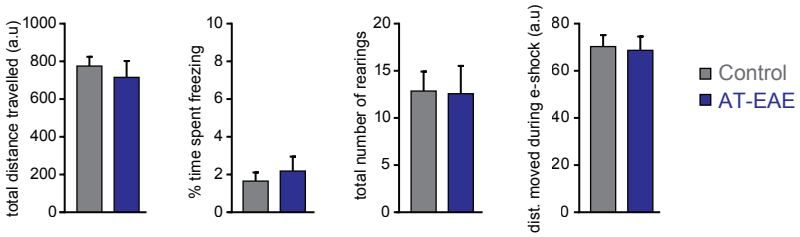

Figure S6 Related to Figure 5

Click here to download Supplemental Figure new Suppl Fig7.pdf

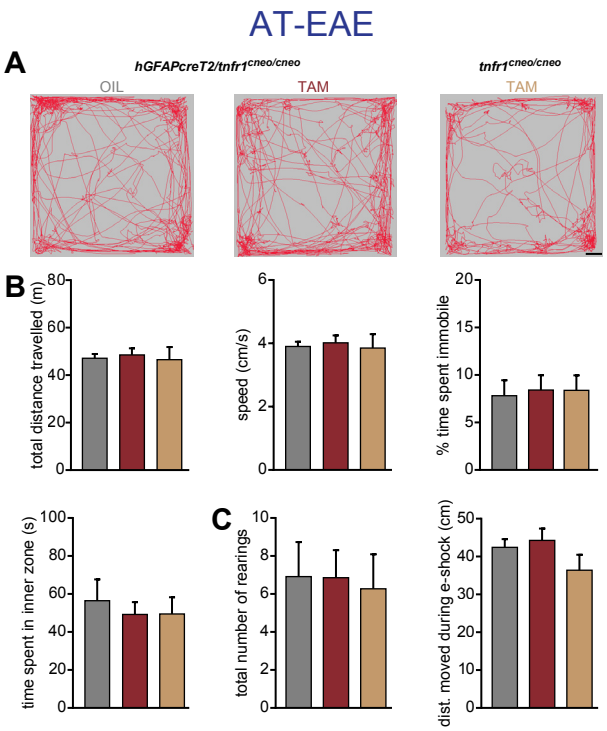

Figure S7 Related to Figure 7